THE ASTROPHYSICAL JOURNAL SUPPLEMENT SERIES, 44:73–110 1980 September

THE UNIVERSE AT FAINT MAGNITUDES. I. MODELS FOR THE GALAXY AND THE PREDICTED STAR COUNTS

JOHN N. BAHCALL AND RAYMOND M. SONEIRA
Institute for Advanced Study, Princeton
Received 1979 August 6; accepted 1980 March 19

CONTENTS

LIST OF FIGURES AND TABLES

ABSTRACT

A detailed model is constructed for the disk and spheroid components of the Galaxy from which the distribution of visible stars and mass in the Galaxy is calculated. The application of star counts to the determination of galactic structure parameters is demonstrated. The possibility of detecting a halo component with the aid of star counts is also investigated quantitatively.

The stellar luminosity functions and scale heights are determined from observations in the solar neighborhood. The global distribution of matter is assumed, based on studies of other galaxies, to be an exponential disk plus a de Vaucouleurs spheroid. The spheroid luminosity function is found to have the same shape as the disk luminosity function over the range of absolute magnitudes (+4 to +12) that contributes significantly to the star counts for $m_V \leq 30$. The density of spheroid stars in the solar neighborhood is 1/800 of the value for the disk. The star counts calculated using the density variation of a de Vaucouleurs spheroid are consistent with the available data; the counts predicted with the aid of a Hubble law are inconsistent with observations at more than the two-sigma level of significance.

The variations of the calculated star densities with apparent magnitude, latitude, and longitude agree well with the available star count data for the observationally well studied range of $4 \lesssim m_V \lesssim 22$. The calculated $(B-V)$ color distributions are also in good agreement with existing data. The color data also indicate that QSOs comprise only a few percent of the total number of stellar objects to $m_V = 22$ ($m_B = 22.5$). The spheroid component is found to be approximately spherical. The scale lengths of the Galaxy model and computed total luminosity and M/L ratios for the disk and spheroid are in agreement with observations of other Sbc galaxies. Illustrative Fig. and a table of interesting characteristics (such as the mass and luminosity contained within various radii and the escape velocity) are provided.

Further ground-based observations at attainable faint magnitudes ($m_V \leq 23$ mag) would be important. Star counts and $(B-V)$ colors in several widely separated selected fields would permit a more accurate determination of the disk scale length and the spheroid star density and ellipticity. The most effective regions in which to make these observations are specified.

The Galaxy model of the disk and spheroid is used to predict the star densities (in B and V) that may be observable with the aid of the Space Telescope down to very faint magnitudes. The stellar density to $m_V = 28$ from the disk and spheroid is predicted to be 10^4 stars per square degree at the galactic pole. The predicted star counts are insensitive to many of the model parameters, although drastic changes in the shape of the luminosity function outside the presently determined magnitude range could produce measurable departures from the predicted star counts at faint magnitudes.

The rotation curve computed solely from the disk and spheroid components decreases beyond about 10 kpc from the center of the Galaxy. A halo with even a relatively small mass density in the Solar neighborhood ($\rho_{\rm Halo}(\odot) = 0.01\ \mathcal{M}_\odot {\rm pc}^{-3}$) can give rise to a flat rotation curve. The stellar content of such a halo would be revealed by observations with Space Telescope cameras if the halo consists of main sequence stars with $M_V{}^{\rm MS} \lesssim 19.0$ mag (existing observations imply $M_V{}^{\rm MS} \gtrsim 14.0$ mag) or faint white dwarfs with $M_V{}^{\rm WD} \lesssim 17.5$ mag (existing observations imply $M_V{}^{\rm WD} \gtrsim 13.0$ mag). Existing data imply $(M/L)_{\rm Halo} \gtrsim 650$ (Solar Visual units).

The results for V magnitudes are described in the main text; the corresponding results for B magnitudes are summarized in Appendix A. A table of predicted differential and integrated star counts for both V and B magnitudes is given in Appendix B. Simple formulae that reproduce to an accuracy of 15% the predicted model star densities as a function of magnitude, latitude, and longitude are also provided in Appendix B.

Subject headings: cosmology — galaxies: internal motions — galaxies: Milky Way — galaxies: stellar content — galaxies: structure

I. INTRODUCTION

We present calculations of the distribution on the sky of stars brighter than 30 mag. The results were obtained with the aid of detailed models of the stellar content of the Galaxy. We show, using these models, how star counts can help determine galactic parameters and how they might reveal, in addition to the distribution of visible stars and mass, the existence of a third stellar component that comprises a massive halo.

Modern ground-based observations aided by computer analyses and future Space Telescope (ST) observations will permit deeper and more accurate star-count surveys to be conducted. We have carried out detailed calculations of what may be observed at the fainter magnitudes that are becoming accessible.

The model results derived here will be useful in helping to recognize, by comparison, unexpected phenomena in future surveys. Also, the calculated sensitivi-

ties of the results suggest ways of determining observationally the values of various parameters, especially those describing the spheroid and halo star densities. The predicted star densities are also needed for estimating the background in ST studies of faint stars (in, e.g., globular clusters) and in calculating guide star accessibility.

This paper is the first in a series of studies that is intended to help indicate the most important capabilities of the ST cameras, to point out key areas in which further ground-based observations are needed, and to assist astronomers in planning future ST observing programs by suggesting which measurements may be most informative. Our ultimate goal is to calculate, with the aid of illustrative models, the number-magnitude relation for various astronomical objects in several colors and directions, down to the limiting magnitudes of the ST cameras. Studies in progress include galaxies, quasi-stellar objects, globular star clusters, and galaxy clusters.

We provide in this paper theoretical calculations of the expected star densities from conventional disk and spheroidal populations as well as from a less well determined massive halo. We explore numerically the uncertainties in these calculations due to various parameter choices and assumptions. We also derive from our models characteristic parameters, dynamical and static, for the Galaxy.

Our Galaxy models differ in purpose and detail from other recent models (see especially the important models of Schmidt 1965; Innanen 1973; de Vaucouleurs and Pence 1978; Ostriker and Caldwell 1978). Our goal is to calculate expected star counts as a function of magnitude, latitude, and longitude, not only the overall distribution of matter or luminosity. We use stellar luminosity functions and scale heights derived from local observations, while the assumed global forms of the density laws are taken from accurate measurements of the light distributions in other galaxies. An authoritative and interesting account of the classical work on star counts is given in *The Distribution of Stars in Space* (Bok 1937).

We show in the present paper that the classical data on star counts in the Visual band are consistent with the adopted simple geometrical model of the Galaxy. The computed and observed star counts agree satisfactorily in the observationally well-studied range, $4 \leq m_V \leq 22$, which corresponds to more than five orders of magnitude variation in the projected star densities at the galactic pole. The model accurately reproduces the observed variation in star counts with latitude ($b^{II} \geq 20°$) and longitude. The distribution of $(B-V)$ star colors calculated from the model is in excellent agreement with data from two widely separated fields at 21st mag. The color data also indicate that QSOs comprise only a few percent of the total number of stellar objects to $m_V = 22$ or ($m_B = 22.5$). The faintest star counts (21 mag$\lesssim m_V \lesssim$23 mag) reported by Tyson and Jarvis (1979) could be indicative of a new stellar population in a massive halo; their work raises important questions (see § III*c* and § VI*b*) requiring further observational study and verification with ground-based telescopes.

We have concentrated our attention in this first study on the Visual and Blue bands. (Work in progress examines star counts in the red *R* and *I* bands.) For the *B* and *V* spectral regions, the required empirical data on stellar densities, scale heights, and luminosities in the solar neighborhood are available, and the theoretical assumptions that underlie the calculations are simple and plausible. The discussion in the main text is limited to the Visual band in order not to complicate the presentation. The corresponding results for the Blue band are presented in Appendix A.

The plan of the paper is described below. The elements of the two-component (disk plus spheroid)Galaxy model are assembled in § II and summarized in Table 1. Motivated by extragalactic as well as galactic observations, we represent the stellar content by an exponential disk plus a de Vaucouleurs spheroid. Luminosity functions and scale heights of disk stars are taken from observations of the solar neighborhood. The spheroid luminosity function is found to have the same shape as the disk luminosity function over the range of absolute magnitudes (+4 to +12) that contributes significantly to the star counts for $m_V \leq 30$. The density of spheroid stars in the solar neighborhood is 1/800 of the value for the disk. Three empirical forms for the galactic obscuration are included in the calculations. The disk and spheroid star distributions that are predicted by the standard model are derived as a function of apparent magnitude and galactic latitude and longitude in § III and compared with the available observations. The model results are consistent with the well-established star counts for galactic latitudes above 20°. The distributions of visible stars in distance, absolute magnitude, and $(B-V)$ color are also presented §III. Simple formulae that reproduce to an accuracy of 15% the predicted model star densities as a function of magnitude, latitude, and longitude are provided. The density variation of a de Vaucouleurs spheroid is consistent with the available data; the Hubble law disagrees with the data at more than the two-sigma level of significance. The sensitivity of the predicted counts to input data is discussed in § IV. The effect of an oblate spheroid component in the counts is examined. The spheroid component is found to be approximately spherical. Uncertainties in the luminosity functions and the parameters that specify the density distributions are considered. Some characteristics of the standard two-component Galaxy model are presented in § V and summarized in Table 4; these include for each component the mass, luminosity, and number of stars ($M_V \leq 19$) within specified radii and their corresponding surface densities, as well as the escape velocity and total disk angular momentum. The rotation curve is computed for the disk plus spheroid, whose masses are

scaled up to take account of the local missing matter. The computed Oort rotation constants A and B are sensitive to the assumed scale length of the disk. However, none of the standard two-component models predicts a flat rotation curve at large distances. The effects of a massive halo are discussed in § VI. It is shown that the rotation curve of the model Galaxy (halo plus disk plus spheroid) can be made to resemble that of other galaxies of approximately the same Hubble type if the distribution of halo mass is assumed to be of the form $\rho_{\rm Halo}(r) \propto [a^2+r^2]^{-1}$. Observational limits on the halo parameters are derived. It is shown, for example, that ST observations can detect the objects making up a massive halo if they are main-sequence–type stars with characteristic absolute magnitudes $M_V \lesssim 19$ mag (or white dwarfs with $M_V \lesssim 17.5$ mag). Some of our main results and several suggested ground-based observations or applications to ST measurements are summarized in § VII. The integral and differential star counts predicted by the standard two-component Galaxy model are summarized in two convenient tables and an approximate analytic formula in Appendix B.

II. THE MODEL OF THE GALAXY

The observed distribution of visible stars in spiral galaxies is described accurately (de Vaucouleurs 1959; Freeman 1970; Kormendy 1977*a*) for most spirals by the combination of a thin exponential disk and a de Vaucouleurs spheroid which has a light distribution similar to that of an elliptical galaxy. We adopt this two component description as the basis of our standard Galaxy model. (The existence of two different stellar components of the Galaxy was first noted by Oort [1926] and, in a different context, by Baade [1944].)

The stellar luminosity functions and scale heights are assumed independent of distance from the galactic center. Data from the solar neighborhood are used to obtain the luminosity function for stars in each component. The spheroid is assumed to consist exclusively of high velocity stars and hence is made up mostly of Population II stars. The empirical model for the disk consists of a broad range of stellar population types, ranging from extreme Population I to Population II.

The spheroidal component is sometimes referred to as a nuclear bulge or a halo. We reserve the term halo for a third stellar distribution of high mass-to-light ratio, discussed in § VI.

a) *The Disk*

All of the local stars are treated as belonging to the disk component since the expected density of (high velocity) spheroidal component stars is extremely small in the solar neighborhood (roughly one in 10^3 stars, see § II*b*, below). The luminosity function of disk stars is determined from star counts as a function of apparent magnitude together with distances to a representative subsample of stars. McCuskey (1966) reviews the various methods utilized in determining the local luminosity function. The generally accepted function appears to have changed little in the 36 years that elapsed between the publication of the papers of Luyten (1938) and Wielen (1974), although it has occasionally been questioned (Weistrop 1972). More recent analyses find no discrepancy between the standard function and the best observational material (Weistrop 1976; Faber *et al.* 1976).

Figure 1 is a plot of the luminosity functions of McCuskey (1966), Luyten (1968), and Wielen (1974).

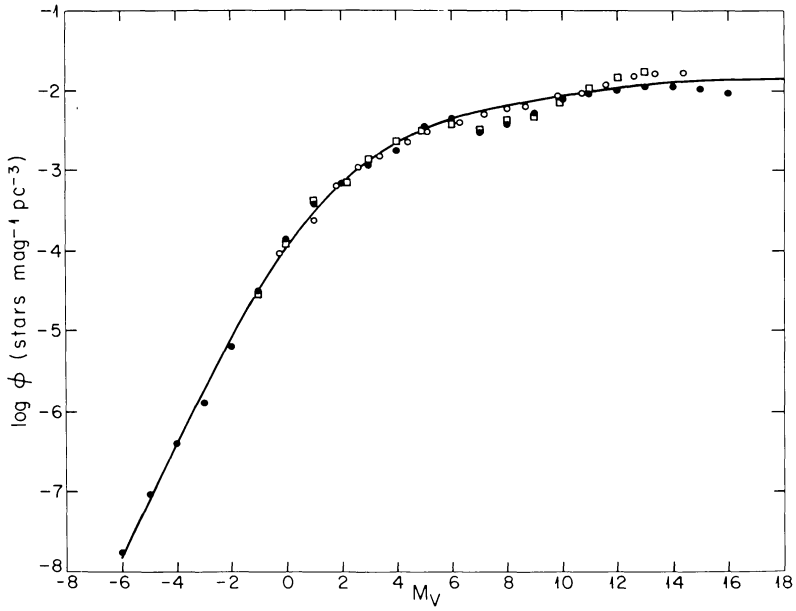

FIG. 1.—Stellar luminosity functions for the disk in the Visual band determined by McCuskey (1966), *filled circles*; Luyten (1968), *open circles*; Wielen (1974), *squares*. The solid line is the analytic approximation given by eq. (1).

(The Luyten data were reduced to the Visual band by Miller and Scalo [1979]). The small dip around $M_V \approx 7$ is not statistically significant and is not found by all observers (see also Fig. 12); the turnover or flattening about $M_V = 14$ does, however, appear to be real. The function is uncertain for $M_V \lesssim -3$ because of the paucity of objects in this range. The satisfactory agreement among the luminosity functions obtained by various observers using different methods (and over long periods of time) suggests that the disk population is adequately known. The dimmest stars plotted in Figure 1 correspond approximately to the lowest possible mass for main-sequence stars ($\sim 0.1 \mathcal{M}_\odot$); the brightest stars plotted correspond to the brightest stars found in very young clusters (Sandage 1957). We discuss below possible errors resulting from the uncertainty of the function for $M_V \lesssim -3$ and $M_V \gtrsim +16$.

For convenience we have fit the data to an analytic luminosity function, $\phi(M)$, of the form (Tremaine, Ostriker, and Spitzer 1975; Soneira 1980):

$$\phi(M) = \frac{n_* 10^{\beta(M-M^*)}}{[1+10^{-(\alpha-\beta)\delta(M-M^*)}]^{\frac{1}{\delta}}}, \quad M_b \le M \le 15,$$

$$= \phi(15), \quad 15 \le M \le M_d,$$

$$= 0, \quad M \le M_b, \text{ or } M \ge M_d, \qquad (1)$$

with

$$n_* = 4.03 \times 10^{-3}, \quad M^* = +1.28, \quad M_b = -6, \quad M_d = +19,$$

$$\alpha = 0.74, \quad \beta = 0.04, \quad \frac{1}{\delta} = 3.40.$$

This function has been plotted as the solid line in Figure 1. The resulting fit of the curve to the data is excellent.

The distribution of stars perpendicular to the plane of the Galaxy varies with luminosity. The typically younger and more massive stars are found relatively close to the plane, whereas the older and less massive stars are not as localized. The variation in star density, $\rho_d{}^{\perp}$, with perpendicular distance z from the plane is given to a good approximation by an exponential function

$$\rho_d{}^{\perp}(z, M) \propto \exp[-z/H(M)], \qquad (2a)$$

with H the scale height. Figure 2 shows the observed variation in scale height with luminosity measured for main-sequence stars from the published data (based, in part, on Miller and Scalo [1979]). The values for the fainter stars ($M_V \gtrsim +8$) are extrapolations; Faber *et al.* (1976) find evidence for an exponential scale height of ~ 300 pc for M dwarfs to $M_V \approx +13$. The adopted relation is shown by the solid line.

Older stars that have evolved off the main sequence may have larger scale heights than the typically younger main-sequence stars. The velocity dispersion of a class of stars is expected to increase with time as a result of collisions with clouds (Spitzer and Schwarzschild 1951). Thus older stars, such as white dwarfs and giants, may have large scale heights. We make the plausible assumption that the white dwarfs, which comprise a few precent of dim stars, $M_V \gtrsim +10$, are themselves distributed like the typically older dim stars, with a scale height $H = 325$ pc (see Fig. 2).

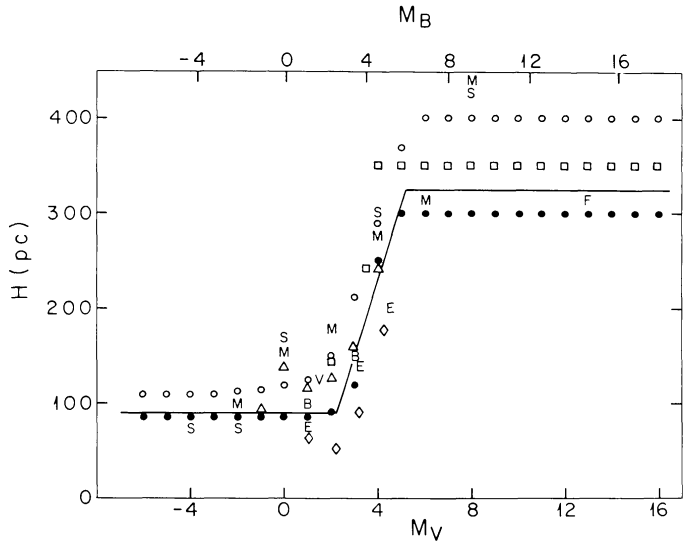

FIG. 2.—The variation in exponential scale height with absolute magnitude measured from the published data of Schmidt (1959), *open circles*; Schmidt (1963), *filled circles*; Oort (1932, 1936), *open squares*; McCuskey (1966), *open triangles*; Upgren (1964), *diamonds*; Becker (1939), B; Elvius (1951, 1965), E; Faber *et al.* 1976, F; Bok and MacRae (1941), M; van Rhijn and Schwassmann (1935), S; van Rhijn (1955), V.

The star counts fainter than about $m_V = 15$ are independent of the uncertainty in the scale heights of the giants, but we briefly review the observations of giants in order to motivate our choice of parameters. There is considerable scatter in the scale heights of late giants ($M_V \approx +1$) as reported in the published data. The most plausible estimate may be 250 pc (Oort 1960), but very different values have been published (150 pc, Elvius [1951, 1965]; 225 pc, Hill [1960]; 300 pc, van Rhijn [1956]). These scale heights could be overestimates because of the increased fraction of nondisk stars encountered at large distances from the Galactic plane (see Blaauw 1965, Table 4). This effect may explain the fact that the star densities for giants fall less slowly than an exponential after a few scale heights (see Elvius 1965, Fig. 1). (The effect is enhanced for the giants because they can be seen to very large distances, and because almost all of the [G-type] nondisk stars are on the giant branch, whereas a much smaller fraction [$\sim \frac{1}{3}$] of the [G-type] disk stars are giants.) Subgiants ($M_V \approx +1$ to $+4$) will have scale heights in between those of the main-sequence stars and the giants. In fact, the subgiants are the most likely to affect the observable star counts, because while the fraction of stars off the main sequence in this magnitude range is quite low (1/3 to 1/10, [Sandage 1957]), the luminosity function, which represents all stars, is much larger in the subgiant region than in the giant region.

In summary, we adopt the relation shown in Figure 2 for all stars. Even if the scale height for giants and subgiants were as large as 250 pc, the star counts in the direction of the galactic pole (§ III) for stars brighter than $m_V = 12$ would increase by less than 20%, whereas there would be essentially no change in the counts for $m_V \geq 15$.

The variation in star density $\rho_d{}^{\parallel}$ with distance x within the plane of the disk for spiral galaxies is approximated by an exponential (de Vaucouleurs 1959; Kormendy 1977*a*)

$$\rho_d{}^{\parallel} \propto \exp[-(x - r_o)/h], \qquad (2b)$$

where r_0 is the distance of the Sun from the galactic center and the scale length h varies with morphological type (Freeman 1970). A similar result is found in H I and CO (Roberts and Whitehurst 1975; Gordon and Burton 1976; Bosma 1978; Knapp, Tremaine and Gunn 1978; Solomon and Sanders 1979). De Vaucouleurs and Pence (1978) suggest $h \approx 3.5$ kpc, based on a plausible value for the central surface brightness of the Galaxy (Freeman 1970), the distance of the Sun from the galactic center, and the total surface brightness of the stars visible from the Sun. The H I observations of Gordon and Burton (1976) yield $h = 3.4$ kpc, and those of Knapp *et al.* give $h = 3.2 \pm 0.6$ kpc. For definiteness, we assume $h = 3.5$ kpc in our standard model. The value of $h = 3.5 \pm 0.5$ kpc is also the mean for Sbc galaxies in the Freeman (1970) sample, where a Hubble constant of 100 km s^{-1}Mpc^{-1} is assumed. The generally assumed morphological type for the Galaxy is Sbc (van den Bergh 1968). For Sb, Sbc, and Sc galaxies the mean value of h is 3.0 ± 1.25 kpc, again assuming a Hubble constant of 100 km s^{-1}Mpc^{-1}. For a Hubble constant of 50 km s^{-1}Mpc^{-1}, an h of 3.5 kpc for the Galaxy is 3 standard deviations from the mean for Sbc type galaxies and 1 standard deviation from the mean for Sb to Sc type galaxies. However, the sample sizes are small, and there may be systematic errors in determining the disk scale lengths from the luminosity profiles. The star counts for the latitudes $b^{II} \geq 20°$ that we consider in this paper do not depend strongly on h (see § III*e* and § IV). The value of h does affect the kinematics of the Galaxy (see the discussion in § V*c* and § VI*a*).

The star density in the disk, ρ_d, is obtained by combining equations (2a) and (2b),

$$\rho_d(\mathbf{r}, M) = \exp[-z/H(M) - (x - r_0)/h]. \qquad (2c)$$

This relation may fail near the galactic center (Kormendy 1977*a*), but our results on observable star densities are not sensitive to the value of ρ_d near $x = 0$ (see § IV*e*).

The luminosity function (eq. [1]), when taken together with the spatial distribution given by equation (2c), completely specifies the disk to the level of detail considered here. The disk number counts (§ III) follow from integrating this model density along the line of sight.

b) *The Spheroid*

The spheroid is an important component of spiral galaxies of morphological type earlier than Sc and shows up in photographs of nearby spiral galaxies of such early types. In our Galaxy, the local density of stars belonging to the spheroid is small because the Sun is far from the center of the Galaxy. Hence the spheroidal component is much less accurately known than the disk component.

The distribution of stars in the spheroidal component of spiral galaxies is very similar to the star distribution in elliptical galaxies (de Vaucouleurs 1959; Kormendy 1977*a*, *b*). The projected surface brightness relation found by de Vaucouleurs is

$$\log_{10} \frac{I(\theta)}{I(\theta_e)} = -3.3307 \left[\left(\frac{\theta}{\theta_e} \right)^{1/4} - 1 \right], \qquad (3a)$$

where θ is the angular distance from the center, and where half the total luminosity is enclosed within θ_e. The de Vaucouleurs expression agrees well with the data on surface photometry and yields a simple form for the three-dimensional spatial density. The spatial density of stars which projects to equation (3a) has

been found by Poveda (1960). An asymptotic expansion accurate for $(r/r_e) \gtrsim 0.2$ has been given by Young (1976):

$$\rho_s(r) = C \frac{\exp\left[-b(r/r_e)^{1/4}\right]}{\left(\frac{r}{r_e}\right)^{7/8}}, \quad (4)$$

where ρ_s is the space density of spheroid stars, C is a normalization constant, b is a constant equal to 7.669, and r_e is the spatial distance that projects to an observed angle θ_e. De Vaucouleurs (1977*a*) and de Vaucouleurs and Buta (1978) find $r_e \approx r_0/3$, with r_0 the distance of the Sun from the center of the Galaxy. Recent determinations of r_0 vary from 7 to 9 kpc (de Vaucouleurs and Buta 1978; Balona and Feast 1974), somewhat smaller than the previously recommended 1966 *IAU* value of 10 kpc. We adopt $r_0 = 8$ kpc. Our results are not sensitive to moderate variations about this value because the lines of sight are far from the galactic center, and the star density is normalized to locally determined values (see § IV*b*).

Other analytic forms have been proposed for the variation of surface brightness in elliptical galaxies and in the spheroidal components of disk galaxies (e.g., Hubble 1930; King 1966; Abell and Mihalas 1966; Oemler 1976). For purposes of comparison with the de Vaucouleurs law, we shall consider also the expression for surface brightness determined by Hubble in his pioneering 1930 study:

$$I(\theta) = I(0) \Big/ \left(1 + \frac{\theta}{a}\right)^2. \quad (3b)$$

The spatial density that projects to this surface density is rather complex (Hubble 1930, eq. [16] and [17]). The Hubble law has a logarithmically divergent luminosity. (Star counts in a magnitude-limited sample are not strongly affected by this divergence.) Many of the alternative formulae are obtained by modifying the Hubble law at large distances in order to eliminate this divergence and to better fit the observed light distributions. At small to intermediate distances, all of the formulae are in good agreement with the data and with each other. In § III*f*, we compare star counts computed using the Hubble and de Vaucouleurs laws; the results favor the de Vaucouleurs expression.

For our standard model, we choose a spheroid component with all three axes equal (i.e., a sphere). Oblate spheroidal models are examined in detail in § IV*d*.

The luminosity function, ϕ (including density normalization), for spheroidal stars in the solar neighborhood has been calculated by Schmidt (1975). Schmidt uses an almost complete sample of 111 stars with measured parallaxes that have large proper motions, i.e., $\gtrsim 1''.3$ per year. From these, he isolates the stars with high transverse velocities >250 km s^{-1}, which almost certainly do not belong to the disk (Oort 1926; Eggen, Lynden-Bell, and Sandage 1962; Oort 1965*b*). (The value 250 km s^{-1} is the median transverse velocity for RR Lyrae stars, so the resulting star densities are doubled by Schmidt in order to correct statistically for the cutoff velocity.) The spheroid sample contains 18 stars. Schmidt calculates the space density using $\Sigma_i[1/V_{m(i)}]$, where $V_{m(i)}$ is the maximum volume out to which a given star i could have been detected. In Figure 3, we compare the integral luminosity function, $\Phi(\leq M) = \int_{+6}^{M} \phi(M)dM$, for the spheroidal stars (*filled circles*) with the integral luminosity function for disk stars from the data of Luyten (1968) (*open circles*). The plotted normalization is arbitrary. *To the accuracy of the data, the two functions have the same shape over the range in common.* This is verified using star count data in § III*d*. In constructing models of the Galaxy, we assume that the shape of the spheroidal and disk luminosity functions are the same over the larger range studied for the disk. This assumption is motivated by the fact that the luminosity function for globular clusters is similar to the function derived for the solar neighborhood in the available data range: $-3 \leq M_V \leq 8$ (see Sandage 1954; Oort and van Herk 1959; Simoda and Hiroshi 1968). (Stars brighter than $M_V = 0$ contribute little to the visible star densities; see Fig. 8*a* of § III*g*.) We discuss in § IV possible errors resulting from the uncertainty of the spheroidal function outside the available data region.

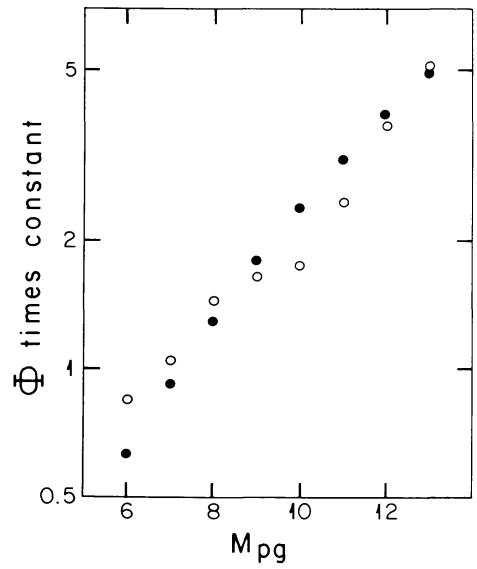

FIG. 3.—The integral luminosity function for the spheroid stars from Schmidt (1975), *open circles*; and for disk stars Luyten (1968), *filled circles*. The relative normalizations are chosen for convenience in display. The two functions have the same shape over the range in common to the accuracy of the data.

The ratio of densities between the disk and spheroidal components is 800:1; thus $n_*(\text{spheroid}) = n_*(\text{disk})/800$ (cf. eq. [1]). This normalization is verified in § IV*d*.

III. DISK AND SPHEROID STAR DISTRIBUTIONS

We derive in this section the expected disk and spheroid star distributions as a function of latitude and longitude. The results are compared with the available observations of star distributions.

a) Basic Relations

The surface number density of stars, $\mathcal{A}_i(m_1, m_2, l, b)$, that have apparent magnitudes in the interval $m_1 \leq m \leq m_2$ in the direction (l, b) per projected area on the sky, $d\Omega$, can be calculated for each component i (d for the disk and s for the spheroid) using the luminosity functions (including variation in overall space density with position) of the disk and spheroidal components specified in §§ I and II. The surface density of stars may be expressed in the form:

$$\mathcal{A}_i(m_1, m_2, l, b)\, d\Omega = \int_{m_1}^{m_2} dm' \int_0^{\infty} dR\, R^2 \rho_i(\boldsymbol{r}, M) \phi_i(M)\, d\Omega, \quad (5a)$$

where

$$\mathcal{A}_T = \mathcal{A}_d + \mathcal{A}_s, \quad M = m' - 5\log R - A(\boldsymbol{R}) + 5,$$

and

$$z = R \sin b,$$

with

$$x = \left[r_0{}^2 + R^2 \cos^2 b - 2 R r_0 \cos b \cos l \right]^{1/2}, \quad (5b)$$

and

$$r = [x^2 + z^2]^{1/2}.$$

Here R is the distance from the Sun, r is the distance from the center of the Galaxy, and A is the total galactic obscuration in the direction (l, b) out to a distance R from the Sun. The star densities, ρ, and luminosity functions, ϕ, are defined by equations (1), (2), and (4). (Unless otherwise specified, (l, b) refer to new galactic coordinates $(l^{\text{II}}, b^{\text{II}})$. We do not distinguish between northern and southern galactic latitudes, i.e., $b = |b^{\text{II}}|$, unless specified otherwise.)

We use three different expressions for the galactic obscuration $A(\boldsymbol{R})$ (no obscuration, the cosecant model, and the Sandage model) in order to take account of the recognized uncertainties in this quantity. Obscuration in the Visual band is small (≤ 0.3 magnitudes) on all models for galactic latitudes $\gtrsim 30°$. The obscuration is patchy; it seems to arise from small dust clouds that may be characterized by a random distribution with a typical scale height of 100 pc with respect to the galactic plane (Spitzer 1978). Even within a few degrees of the galactic center there are "Baade windows" (Baade 1951) where the obscuration to the center is as low as 1.4 mag (Arp 1965; van den Bergh 1971). This results in fluctuations in the observed star counts (see below) and complicates the derivation of simple models for $A(\boldsymbol{R})$.

The classical model of a uniform semi-infinite obscuring layer gives the obscuration $A_\infty(b)$ for an object completely outside the layer (denoted by the subscript ∞) with latitude b as

$$A_\infty(b) = A_\infty(90°) \csc b. \quad (6)$$

The constant for obscuration at the pole, $A_\infty(90°)$, is 0.15 magnitudes in the Visual band (de Vaucouleurs, de Vaucouleurs, and Corwin 1976), with $A_V = 0.75 A_B$ (Morgan, Harris, and Johnson 1953; Heiles 1976). Sandage (1972) modified the cosecant law in order to account for the very small reddening measured at high galactic latitudes. The obscuration relation proposed by Sandage is

$$A_\infty(b) = 0.165\,(1.192 - \tan b) \csc b, \quad b \leq 50°,$$
$$= 0, \quad b > 50°. \quad (7)$$

Some studies have confirmed the small reddening near the poles (see Burstein and Heiles 1978), but the issue is still in dispute (see de Vaucouleurs, de Vaucouleurs, and Corwin 1976).

We have assumed an exponential variation of the density of the obscuring layer with height z above the galactic plane, $\rho = \rho_0 \exp(-z/H)$, where the scale height $H = 100$ pc (see above). Any possible variation with distance from the galactic center is neglected. The obscuration A is then

$$A(\boldsymbol{R}) = A_\infty(b)[1 - e^{(-\sin b/H)R}]. \quad (8)$$

If the cloud density changes with distance from the galactic center in a manner similar to the disk star density (eq. [2b]), then $A(\boldsymbol{R})$ will be significantly affected for $b \lesssim 10°$. We neglect this possible variation because the strong and patchy obscuration at such small galactic latitudes prevents visible star counts from being very useful for galactic studies.

The characteristics of our standard model of the Galaxy are summarized for convenience in Table 1. We have calculated the disk and spheroid star distributions predicted by this model using equation (5) and the parameters summarized in Table 1.

TABLE 1

THE STANDARD GALAXY MODEL

Characteristic	Disk	Spheroid
Luminosity Function . . .	$\frac{4\times10^{-3}\times10^{0.04(M-1.3)}}{[1+10^{-0.2(M-1.3)}]^{3.4}}$ [a]	Disk Luminosity Function/800
Geometrical Scales	$\rho_d{}^{\perp}\propto e^{-z/H(M)}$ [b] $\rho_d{}^{\parallel}\propto\exp[-(x-8)/3.5\ \mathrm{kpc}]$ [c]	Deprojection of $\log I(\theta)\propto[(\theta/\theta_e)^{1/4}-1]$ $r_e=2.7$ kpc [d]
Obscuration Models	$\begin{cases} A=0 \\ A=0.15\csc b \\ A=0.17(1.2-\tan b)\csc b \end{cases}$ $\rho_{\mathrm{obs}}(z)=\rho_{\mathrm{obs}}(0)\exp-(z/0.1\ \mathrm{kpc})$	

[a] See equation (1).
[b] See Figure 2.
[c] See equation (2).
[d] See equation (4).

b) Observed Counts

The most comprehensive set of observations of star densities, reduced and calibrated to a single standard system, is still that of Seares *et al.* (1925). Their work is based primarily on counts of $\sim10^5$ stars with measured magnitudes, from the *Mount Wilson Catalogue of Selected Areas*. This catalog consists of 139 selected areas each about $1/3°\times1/3°$ in size; the magnitude range covered is $m_V=+13$ to $+18$. For stars brighter than +13 mag, Seares *et al.* use a number of other star catalogs, principally the *Astrographic Catalogue*. Seares *et al.* smoothed their tabulated star counts using a third-order polynomial to take out the fluctuations. Seares *et al.* list star counts as a function of latitude only (i.e., averaged over all longitudes) in the international photographic band. The variation with longitude was studied by Seares and Joyner (1928).

Counts in the Visual band, m_V, can be obtained from those given in the international photographic band, m_{ipg}, with the aid of the relation found by Seares (1925)

$$m_V=m_{\mathrm{ipg}}+c,$$
$$c=-0.16-0.05m_{\mathrm{ipg}}. \qquad (9)$$

This relation is an average over latitudes 0°–90°; the variation of color with latitude was not determined, but is expected to be small over the range of latitudes considered in this paper. The standard model predicts that the variation in color between latitudes 20° and 90° is 0.10 mag (see § III*h*). (This figure is an average over all longitudes, for use with the Seares *et al.* [1925] data. There is, however, a considerable variation in color with longitude, e.g., at latitude 20° the variation is 0.40 magnitudes between $l=0°$ and 180°.)

Photoelectric photometry by Stebbins, Whitford, and Johnson (1950) has indicated a scale error in the original *Mount Wilson Catalogue* magnitude scale. The relation for corrected magnitudes $m_{\mathrm{ipg}}{}'$ is approximated by

$$m_{\mathrm{ipg}}{}'=m_{\mathrm{ipg}}+0.08(m_{\mathrm{ipg}}-13),\ m_{\mathrm{ipg}}\geq13,$$
$$=m_{\mathrm{ipg}},\ m_{\mathrm{ipg}}\leq13, \qquad (10)$$

to better than ±0.2 magnitudes. Assuming that the magnitude scale change is the same in visual and photographic magnitudes and combining equations (9) and (10), we have

$$m_V=1.03m_{\mathrm{ipg}}-1.20,\quad m_{\mathrm{ipg}}\geq13,$$
$$=0.95m_{\mathrm{ipg}}-0.16,\quad m_{\mathrm{ipg}}\leq13. \qquad (11)$$

Automated methods have been used recently to detect, classify, and measure objects on deep photographic plates in order to obtain catalogs of galaxies to faint limiting magnitudes. Faint star counts have been derived as incidental by-products of these extragalactic studies. We summarize the results of Kron (1978) (hereafter called the Berkeley counts), which include $\sim10^{3.4}$ stars; Tyson and Jarvis (1979, hereafter called the Bell Labs counts), including $\sim10^{4.3}$ stars; and Peterson *et al.* (1979, hereafter called the AAT counts), including $\sim10^{2.9}$ stars. The data consist of a few small fields near one of the galactic poles, except for the Bell Labs data, which include several fields with latitudes of 25°–50°. The Berkeley counts refer to $b^{\mathrm{II}}=86°$. The AAT counts refer to $b^{\mathrm{II}}=65°$, but with a longitude of ~90° away from the galactic center so they have about the same normalization as for the pole, $b^{\mathrm{II}}=90°$. The Bell Labs counts are (surprisingly) independent of galactic latitude. The three fields with $b^{\mathrm{II}}\geq74°$ have

the same mean counts to $m_J=24$ as the five fields with latitudes $|b^{II}|$ from 25° to 45°. Therefore in comparing the published Bell Labs data (which are presented as an average over all fields) to the model counts at the galactic pole, we do not scale the data to take into account the range in latitude of the fields observed. The Bell Labs and AAT counts refer to the J-band (between B and V); the Berkeley data include results for the F band (between V and R) as well as the J-band. We use color equations from Kron (1978):

$$m_V=m_J-0.75,$$

$$m_V=(m_J+m_F)/2-0.20, \quad (12)$$

with $(B-V)\equiv(m_B-m_V)=1.0$. This value of $(B-V)$ is expected from the dominance of late dwarfs in the model counts (see § IIIh and Fig. 8c) and is also the mean value found by Kron (see his Figs. 20 and 21). All three of the surveys described above reach a faintest magnitude $m_J=24$. We use the Berkeley and AAT data only to $m_J=22.5$. For magnitudes fainter than 22.5 mag, the magnitude scale for the Berkeley data is distorted by effects of noise and possibly contaminated by galaxies (Kron 1978). For $m_J>22.5$, the AAT data are contaminated by compact galaxies, merged images, and possible QSOs, according to Peterson *et al.* (1979). We discuss the faint end of the Bell Labs data in § IIIc. The Berkeley data begins at $(m_J+m_F)/2=20$, the Bell Labs data at $m_J=13$, and the AAT data at $m_J=18$.

c) *Calculated Versus Observed Star Distributions*

In Figure 4a, we plot the calculated differential star densities $\mathcal{A}(m)$ per square degree per magnitude ($m_1=m-0.5$, $m_2=m+0.5$; eq. [5]) averaged over longitude (see below) that were obtained with the standard Galaxy model of Table 1. Results are shown for galactic latitudes 20°, 30°, 50°, and 90°. For latitudes 20° and 30°, the absorption was calculated using the cosecant model (eq. [6]) with $A_\infty(90°)=0.15$ mag. (At these lower latitudes, there is little difference between the obscuration calculated using eq. [6] or [7]). The dashed line in the figure indicates the calculated star densities at latitude 20° for $A=0$. Let δm be the magnitude offset due to obscuration where δm is defined such that with obscuration $\mathcal{A}(m+\delta m)_{wo}$ equals $\mathcal{A}(m)_{no}$, for no obscuration. Then $\delta m(b=20°)\approx 0.3$ mag (see Fig. 4a). For latitudes of 50° and 90°, the curves shown were calculated for zero obscuration. The calculated effect of obscuration at these latitudes is small using any of the three previously discussed models of the absorbing material (see § IIIa), i.e., $\delta m(b=50°)\lesssim 0.2$ mag.

The observations are compared with the model results in Figure 4a. At large galactic latitudes, the agreement between the model results and the data is excellent to 22nd magnitude. For $m_V\geq 22$ mag, the Bell Labs counts rise much more rapidly than those of the model. This rapid increase in counts (roughly like $10^{0.4m}$) could be due to stars in a distinct halo component (see § VI), or it could arise from a sharply increasing number of QSOs (see § IIIi). There are also other possibilities (including systematic error). The Berkeley and AAT data, which the authors indicate may be contaminated by galaxies near their survey limits, do not increase nearly as rapidly for magnitudes fainter than $m_V=22$. Further observational work on the star density at the galactic pole is required before one can be sure of the correct interpretation of the Bell Labs counts at faint magnitudes.

Brown (1979) has measured the integrated star counts at selected B magnitudes for 12 fields which have latitudes $b\geq 70°$. There are $10^{4.0}$ stars in his sample. These data are compared to the model B counts in Figure 13b. The plotted model counts at the pole are 11% smaller than the mean model counts for the 13 fields in the Brown sample. The agreement is excellent.

At the lowest galactic latitude considered in Figure 4a, $b=20°$, there is about a 0.3 mag offset between the data of Seares *et al.* (1925) and the results of the standard model (using a cosecant obscuration law). The Galaxy model without obscuration fits the data well. There are many possible explanations for this discrepancy. One simple and plausible explanation is that there is an offset in the magnitude scales between high and low galactic latitudes. In the early part of this century it was difficult to transfer the zero point of the magnitude system to regions of the sky that are far from the standard stars of the north polar sequence, which define the system used by Seares *et al.* (1925). A magnitude offset at low galactic latitudes could also arise if we have overestimated the obscuration. The obscuration determined by Sandage (1973) and by Sandage and Visvanathan (1978) is a factor of 2–3 smaller at low galactic latitudes than the values adopted in equations (6) or (7) for the standard model. If the obscuration is this small, the discrepancy at low latitudes noted above disappears. Other possibilities are that we have made a slightly incorrect parameter choice in the model or that a basic assumption in the model is violated to some extent (e.g., the stellar luminosity function may, and probably does, change with position in the Galaxy). There is also the possibility of a sampling error: the solar neighborhood may not be representative of the large volume included in the counts. Note also that the Selected Areas are centered on bright 8th or 9th mag stars. Since the obscuration is patchy (see the discussion on fluctuations of the counts with longitude, below) the existence of bright stars may indicate that the Selected Areas (SA) are regions in which the obscuration is uncharacteristically small. Seares *et al.* (1925) note also that there may be systematic effects on the counts at low galactic latitudes because the distribution of fields in galactic longitude

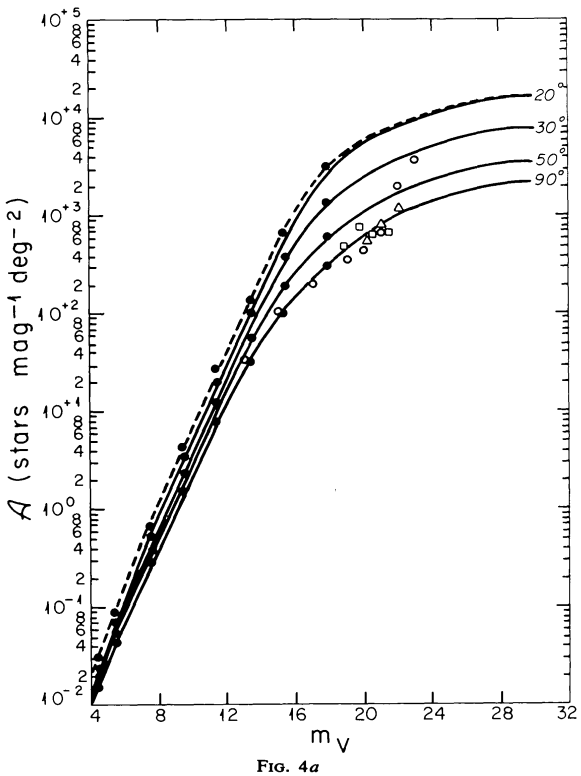

FIG. 4a

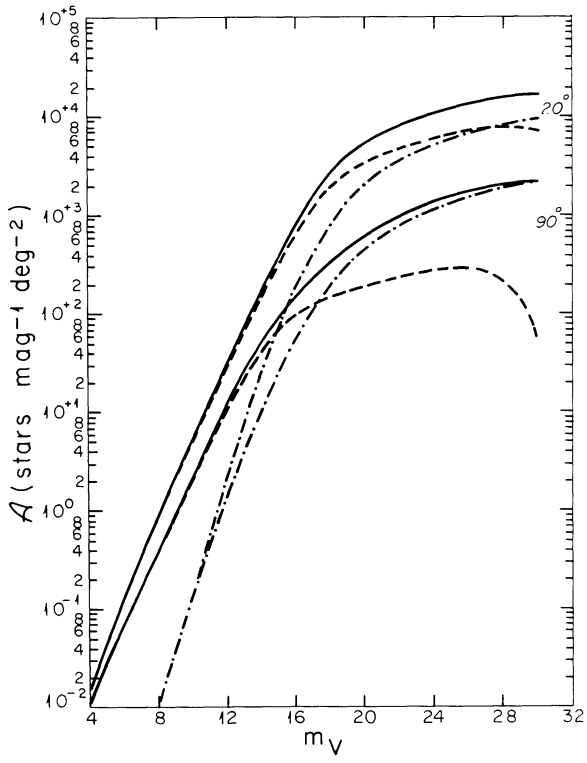

FIG. 4b

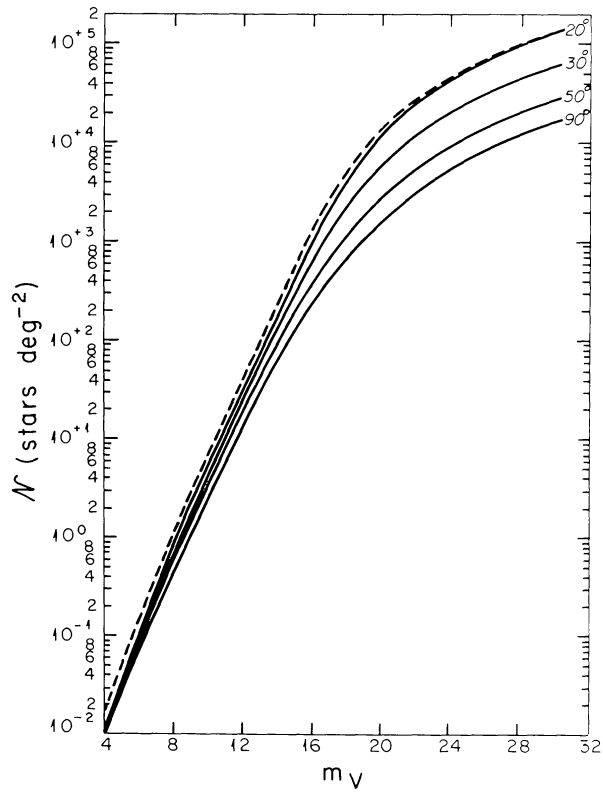

FIG. 4c

FIG. 4.—(*a*) Calculated differential star densities $\mathcal{A}$ mag^{-1} degree^{-2}, averaged over longitude for latitudes b of 20°, 30°, 50° and 90°. The dashed line for $b=20°$ was calculated assuming no obscuration. For latitudes b for 20° and 30°, the solid lines indicate the calculated star densities for a cosecant obscuration model (eq. [6]) with $A_\infty(90°)=0.15$. For latitudes b of 50° and 90°, the densities were calculated assuming zero obscuration. Data from Seares *et al.* (1925), with the magnitude-corrections of eq. (11), are plotted as filled circles. Data from Kron (1978) are plotted as triangles, data from Tyson and Jarvis (1979) as open circles, and data from Peterson *et al.* (1979) as squares. All include the magnitude conversion of eq. (12). (*b*) Calculated differential star densities $\mathcal{A}$ mag^{-1} per square degree averaged over longitude for latitudes b of 20° (cosecant obscuration, eq. [6]) and 90° (no obscuration). Contributions of the disk (*dashed lines*) and spheroid (*mixed dots and dashes*) to the total differential star densities (*solid lines*) are indicated separately. (*c*) Calculated (integral) star densities $\mathcal{N}(\leq m)$ brighter than magnitude m degree^{-2} for latitudes b of 20°, 30°, 50°, and 90°. The dashed line for $b=20°$ was calculated assuming no obscuration. For latitudes b of 20° and 30°, the solid lines indicate the calculated star densities for a cosecant obscuration model (eq. [6]) with $A_\infty(90°)=0.15$. For latitudes b of 50° and 90°, the densities were calculated assuming zero obscuration.

are not representative. As a final alternative explanation, we note that if the scale length of the disk in the plane h is changed to 3 kpc, then the model with a cosecant obscuration law (eq. [6]) fits well the Seares *et al.* (1925) data down to a latitude of 20°. Given the plethora of above-mentioned possible explanations, no detailed conclusions seem warranted on the basis of the small magnitude offset that exists at $b=20°$ between the available data (which are subject to systematic uncertainties) and the standard model.

Figure 4*b* displays the contributions of the disk (*dashed lines*) and spheroid (*mixed dots and dashes*) to

the total differential star densities, $\mathcal{N}_T$, (*solid lines*) for latitudes 20° and 90°. At the galactic pole, the differential counts are dominated by the disk component for $m \lesssim 16$ and by the spheroidal component for $m \gtrsim 19$; the disk and spheroidal densities are equal at 17th magnitude. (For the integral counts, the corresponding values are about 2 mag dimmer.) The thinness of the disk resulting from the exponential fall in density with height above the plane becomes increasingly apparent for magnitudes $\gtrsim$ 17. Beyond 26th mag, the calculated disk counts decrease, corresponding to the effective "edge" of the disk. (The decrease results from the luminosity function, ϕ, being zero for $M > M_d = +19$ (eq. [1]). If $M_d = +\infty$, $\mathcal{N}_D$ remains constant for $m \geq 26$.) At a latitude of 20°, the counts averaged over longitude remain dominated by disk stars about 4 magnitudes fainter than at the galactic pole.

The integrated star densities per square degree, $\mathcal{N}(\leq m)$, (defined as $\mathcal{N}$ with $m_1 = -\infty$, $m_2 = m$) are shown in Figure 4*c* for latitudes 20°, 30°, 50°, and 90°. The obscuration was treated as in Figure 4*a*. The expected integrated star densities at 28th mag vary from 1×10^4 per square degree at the galactic pole to 1×10^5 per square degree at $b = 20°$. The integrated star densities are tabulated in Appendix B for several different latitudes and longitudes.

The variation of the calculated differential star density, $\mathcal{N}(m)$, averaged over longitude is shown in Figure 5 for latitudes $b \geq 20°$. All star densities in Figure 5 were obtained with the aid of the cosecant model (eq. [6]) with $A_\infty(90°) = 0.15$ mag.

The star counts vary significantly with longitude. In Figure 6*a*, we have plotted the differential star densities $\mathcal{N}$ as a function of longitude for latitudes 20°, 30°, 50°, and 70° (using cosecant obscuration, eq. [6]), for latitudes 20° and 30°, and zero obscuration for latitudes 50° and 70°). The variation in density is largest for the lower latitudes and the dimmer magnitudes: for 28th mag stars at latitude 20°, the variation is more than 15/1. In Figure 6*b*, the density variation with longitude has been plotted for the disk and spheroid components separately for latitudes 30° and 50° at 18 and 28 mag. Most of the variation in the star densities with longitude is seen to arise from the spheroid.

The strong longitudinal dependence of the spheroid component in the faint counts (Fig. 6*b*) provides a valuable observational method of measuring more accurately the spheroid star density. A determination of the longitudinal dependence of the differential star counts at about latitude 50° in the range $18 \lesssim m_V \lesssim 22$ mag would be an especially useful constraint on the spheroid component (§ III*f* and § IV*d*; see § III*e* below for the implications of such a measurement for the determination of the disk scale length).

The dependence of the star counts on longitude observed in the available data (Seares and Joyner [1928], Table 15 and Figs. 9–13) is noisier than the theoretical

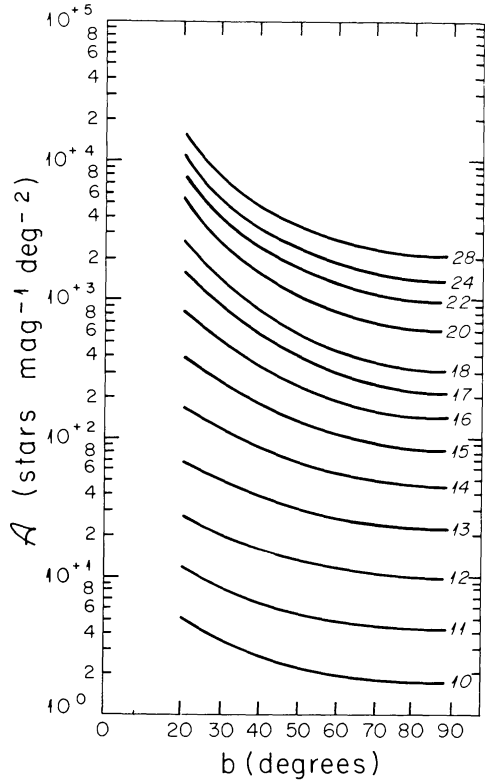

FIG. 5.—The variation of calculated differential star densities $\mathcal{N}$ with latitude b for the indicated magnitudes m_V. All densities were calculated with a cosecant obscuration model (eq. [6]) with $A_\infty(90°) = 0.15$.

results shown in Figure 6. There are even significant differences between galactic hemispheres. The observed fluctuations arise from patchy obscuration, from intrinsic variations in the stellar distribution (star clustering), and from the limited sample represented in the data. We have compared our calculated longitudinal dependences with the observed counts averaged over large (45°) angular regions as tabulated by Seares and Joyner (1928) in terms of logarithmic residuals, $\Delta = \log \mathcal{N} - \langle \log \mathcal{N} \rangle$. In Table 2, we give the logarithmic residuals for the model and the data for latitudes 60° and 20° for magnitudes 12 and 18. (The position of the galactic center in old coordinates is $l^{\mathrm{I}} = 328°$.) The agreement is good. (Note that fluctuations for $m = 12$ are larger because of the small number of stars actually counted.)

d) *Determination of the Spheroid Luminosity Function From Star Counts*

The spheroid luminosity function can be determined directly from the available data on star counts for magnitudes dimmer than $m_V = +18$. The data sample we use extends to $m_V = +22$ in the direction of the galactic pole. For this direction and magnitude interval, the spheroid contributes 70% of the star counts (see

Fig. 4*b*) in the standard model. This method of determining the spheroid luminosity function is independent of, and complementary to, Schmidt's (1975) original determination using high velocity stars. For a given apparent magnitude interval, $m_1 \leq m \leq m_2$, only stars within a range of absolute magnitudes, $M_1 \leq M \leq M_2$, make an appreciable contribution to the star counts (§ III*g* and Fig. 8*a*, below). The logarithmic slope of the luminosity function can be determined for this range of absolute magnitudes.

A power-law luminosity function of the form $\phi(M) = 10^{\gamma M}$, causes the spheroid star counts to increase with magnitude as $10^{\gamma m}$, (eq. [5]), *independent* of the form of the density function, $\rho_s(r)$, assumed for the spheroid, provided only that the function ρ is independent of absolute magnitude. (This result is also valid to the accuracy permitted by the observational data [see below] if the luminosity function is cut off smoothly outside the range of absolute magnitudes $M_V = +3$ to $+9$, which contribute most of the star counts in the apparent magnitude range considered.)

We estimate γ from the available star count data at the galactic pole between $m_V = 18$ and $m_V = 22$. (For this calculation, we ignore the abrupt increase in the Bell Labs data for $m_V \geq 22$, because this feature cannot be associated with the spheroid component.) In order to calculate the spheroid counts, we subtract the disk counts predicted by the standard model from the data. (The spheroid counts could be obtained directly if the $[B-V]$ colors are measured; see § III*h*.)

We weight the data from all observers equally (see § III*b*). We obtain $\gamma = 0.145 \pm 0.035$ (standard deviation) from a least squares fit to the differential star counts. For the apparent magnitude range considered, $18 \leq m_V \leq 22$, 85% of the spheroid stars have absolute magnitudes in the interval $M_V = +4$ to $+8$. The value of γ given above is in agreement with a slope γ of 0.130 determined from the Schmidt (1975) data plotted in Figure 3.

The slope, α, of the stellar mass function $dF/d\mathcal{M} = C\mathcal{M}^{-\alpha}$ can be determined from the value of γ together with (the slope of) the stellar mass-luminosity relation. From the mass-luminosity relation given by equation (17) (see below), we obtain $\alpha = 2.55 \pm 0.37$ for $\gamma = 0.145 \pm 0.035$. This value of α is to be compared with an α of 2.40 for the mass function of disk stars in the same absolute magnitude interval of $+4$ to $+8$. (The mass range corresponding to the above absolute magnitude interval is approximately $0.5-1.0\ \mathcal{M}_\odot$.) Schmidt's original estimate for the value of α based on his data is 2 with an uncertainty of the order of ± 0.5.

e) *Approximate Behavior of the Disk Star Counts*

The variation in disk counts with latitude and longitude has a simple form for bright apparent magnitudes ($m \lesssim 12$) and for dim apparent magnitudes ($m \gtrsim 20$). The counts in these magnitude intervals are dominated, respectively, by the bright and dim ends of the stellar luminosity function, ϕ, (eq. [1] and Fig. 1). (For the derivation of the approximate formulae in this subsection, we assume that the luminosity function has no dim end cutoff, i.e., $M_d = +\infty$, and neglect obscuration.) We approximate, for simplicity, the luminosity function by a power law, $\phi \propto 10^{\gamma M}$, and assume an average scale height $\langle H \rangle$ for the disk (eq. [2c]). Then from equation (5), we find

$$\mathcal{N}_{\rm disk} \propto \frac{10^{\gamma m}}{\left[\sin b \left(1 - \frac{\langle H \rangle}{h} \cot b \cos l\right)\right]^{3-5\gamma}}. \quad (13a)$$

For $m_V \lesssim 12$, $\mathcal{N}$ is dominated by stars with absolute magnitudes $M \lesssim +4$ (see Fig. 8*a* in § III*g*, below). From Figure 1, $\gamma \approx +0.4$, and from Figure 2, $\langle H \rangle \approx 100$ pc. For $m_V \gtrsim 20$, $\mathcal{N}$ is dominated by stars with absolute magnitudes $M \gtrsim +4$ (see Fig. 8*a* in § III*g*, below). From Figure 1, $\gamma \approx +0.04$, and from Figure 2, $\langle H \rangle \approx 300$ pc.

Equation (13a) reproduces to an accuracy of order 10% the predicted variation of $\mathcal{N}$ with l and b (and of order 20% with m) when the above values of γ and $\langle H \rangle$ are used in the magnitude ranges $4 \leq m_V \leq 12$ and $20 \leq m_V \leq 28$.

The determination of the disk scale length from star counts can be discussed most easily with the aid of equation (13a). For bright apparent magnitudes, $\mathcal{N} \propto \csc b$; there is only a small dependence ($\lesssim 10\%$) of the star counts on longitude l and disk scale length h (in the range $b \geq 20°$ and $h \geq 2.5$ kpc). For dim apparent magnitudes, $\mathcal{N} \propto \csc^3 b$, with a dependence on l and h that is approximately nine times larger than for the bright apparent magnitudes. Hence the disk scale length is best determined at dim magnitudes, $m_V \gtrsim +20$, in low to intermediate galactic latitudes, $20° \lesssim b \lesssim 40°$, for which the obscuration is not too large. The most suitable longitudes are $l \gtrsim 120°$, for which the contribution to the star counts by the spheroid is moderately small.

f) *Approximate Behavior of the Spheroid Star Counts and the Spheroid Mass Distribution*

The variation in spheroid star counts with latitude and longitude can be expressed also in a moderately simple form. We suppose the luminosity function is approximately a power law $\phi \propto 10^{\gamma M}$ with $M_d = +\infty$ and neglect obscuration. Then from equation (5), one finds

$$\mathcal{N}_{\rm spheroid} \approx C \frac{10^{\gamma m}}{(1 - \cos b \cos l)^{(\nu-1)/2}}, \quad (13b)$$

where the spatial density of stars is assumed to vary as $r^{-\nu}$, r being the distance from the galactic center.

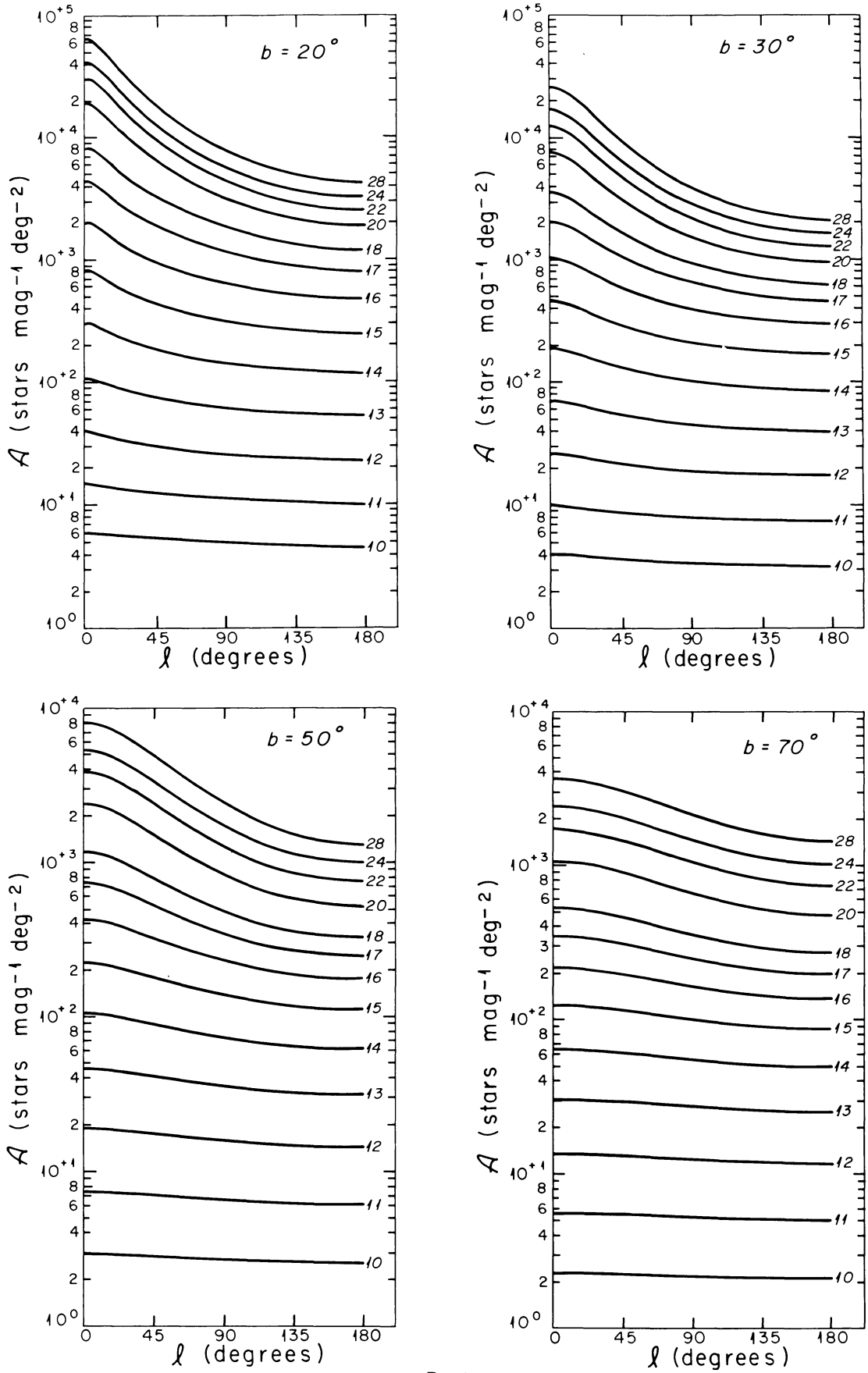

FIG. 6a

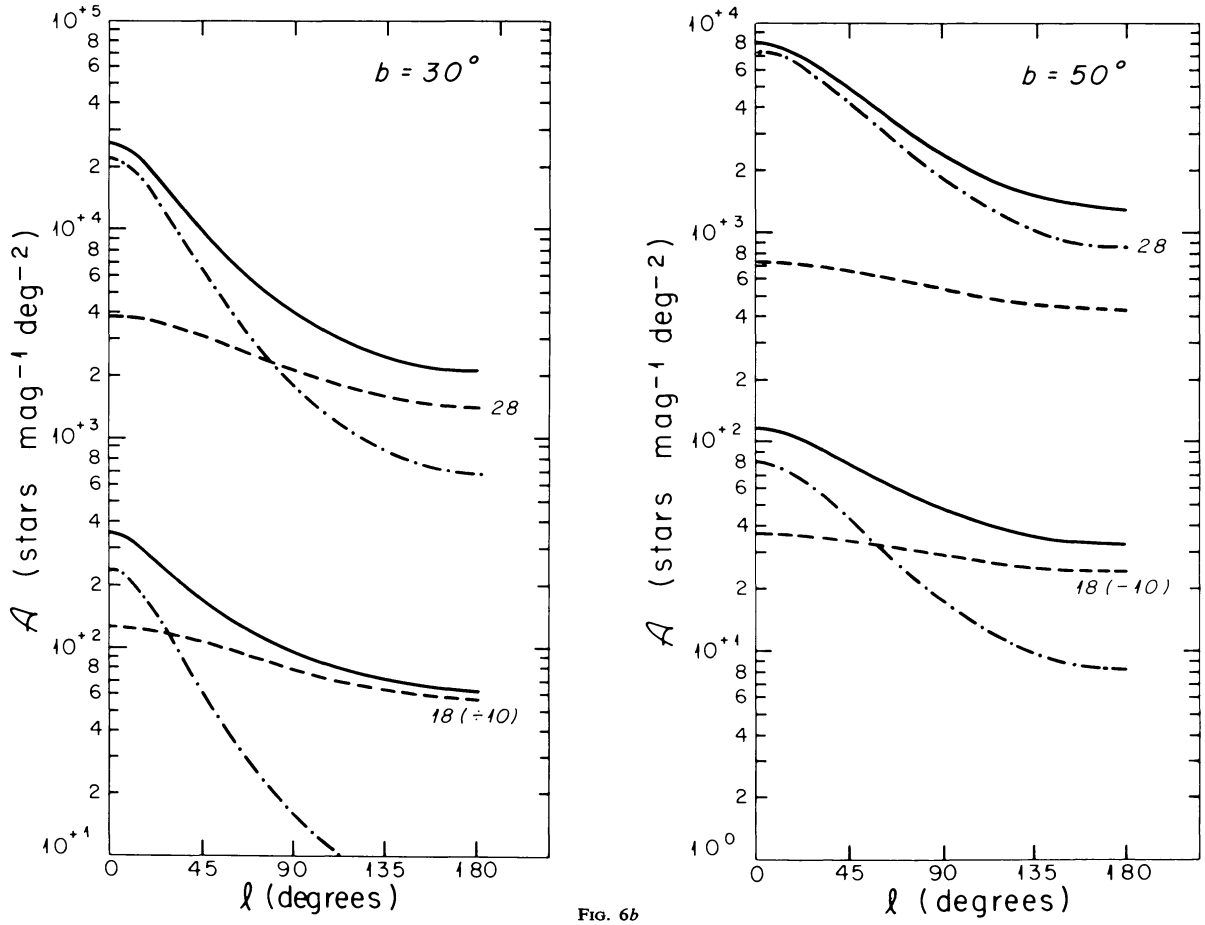

FIG. 6b

FIG. 6.—(*a*) The variation of calculated differential star densities $\mathcal{A}$ with longitude for latitudes b of 20°, 30°, 50°, and 70° for the indicated magnitudes. For latitudes b of 20° and 30°, a cosecant obscuration model (eq. [6]) with $A_\infty(90°)=0.15$ has been used; for latitudes 50° and 70°, the obscuration was set equal to zero ($A=0$): (*b*) The variation of calculated differential star densities $\mathcal{A}$ with longitude for latitudes b of 30° and 50° and magnitudes 18 and 28. For $b=30°$, the star densities are calculated for a cosecant obscuration model (eq. [6]) with $A_\infty(90°)=0.15$; for $b=50°$, the densities were calculated assuming zero obscuration. Contributions of the disk (*dashed lines*) and spheroid (*mixed dots and dashes*) to the total differential star densities (*solid lines*) are indicated separately. The star densities for 18th mag have been divided by a factor of 10 for convenience in display.

Equation (13b) is valid for ν in the observationally relevant range $\nu=4$ (and $\gamma=0.0$–0.3) to $\nu=3$ (and $\gamma=0.1$–0.2). Typical accuracies are better than 10% for $\nu=4$ and better than 20% for $\nu=3$. The constant C depends on ν and γ, and may be calculated by fixing the space density of stars in the solar neighborhood to be equal to the Schmidt (1975) values determined in § II*b*, above. (Oort [1938] studied the spheroid spatial star density distribution by examining deviations from a simple plane-parallel distribution expected for a uniform plane-parallel disk.)

The spatial density of stars in both a de Vaucouleurs spheroid and a Hubble spheroid are well approximated by a power law in distance from the galactic center, $r^{-\nu}$, over the distance ranges examined from the solar position in magnitude limited surveys. In the Hubble spheroid, $\nu=3$ for all directions considered in this paper (≥ 20 degrees from the galactic center). For any direction on the sky more than 50° from the galactic center (as seen from the Sun) the de Vaucouleurs spheroid gives $\nu\approx 3.8$. For directions nearer to the center, the effective ν for the de Vaucouleurs spheroid decreases monotonically until the density varies much like the Hubble law with $\nu\approx 3$ (see Appendix B).

The parameters C and ν could be determined from the variation in star counts with angular distance from the galactic center. The most useful observations are those carried out along the $l=0°$ to $l=180°$ plane since the contamination from disk stars is least for those directions.

The major limitation of equation (13b) is caused by the fact that the logarithmic slope, γ, of the luminosity function is not constant over the entire range of absolute magnitudes that contribute to the spheroid star

TABLE 2

VARIATION IN COUNTS WITH LONGITUDE

l^{II}	$\Delta^a(m=12)$ Data	$\Delta^a(m=12)$ Standard Model[b]	$\Delta^a(m=18)$ Data	$\Delta^a(m=18)$ Standard Model[b]
		$b^{II}=60°$		
0°–45°, 315°–360°	0.04	0.03	0.12	0.15
45°–90°, 270°–315°	0.01	0.01	0.03	0.03
90°–135°, 225°–270°	−0.03	−0.02	−0.04	−0.06
135°–180°, 180°–225°	−0.02	−0.02	−0.09	−0.12
		$b^{II}=20°$		
0°–45°, 315°–360°	0.04	0.07	0.28	0.32
45°–90°, 270°–315°	0.10	0.01	0.06	0.03
90°–135°, 225°–270°	−0.01	−0.03	−0.09	−0.13
135°–180°, 180°–225°	−0.14	−0.06	−0.23	−0.21

[a]The tabulated quantity is $\Delta = \log \mathcal{N} - \langle \log \mathcal{N} \rangle$.

[b]Standard Galaxy model refers to the model defined in Table 1 with $A=0$. Galactic obscuration is unimportant at the level of accuracy considered here (appropriate to the available data).

counts (see Fig. 8*a* in § III*g*, below). Hence we rely on direct numerical integration of equation (5) for accurate measurements of ν.

We have made an approximate determination of ν using the presently available deep star counts at the galactic pole. Because there are data for only one direction, it is necessary to rely on the variation of $\mathcal{N}$ with apparent magnitude alone. We use available data in the magnitude interval $18 \leq m_V \leq 22$. (We do not include in this analysis the abrupt increase in the Bell Labs data for $m_V \geq 22$, because this feature cannot be associated with the spheroid component.) We subtract

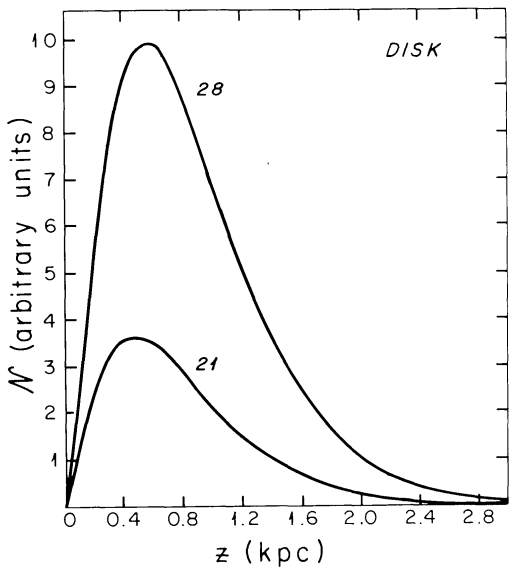

FIG. 7*a*

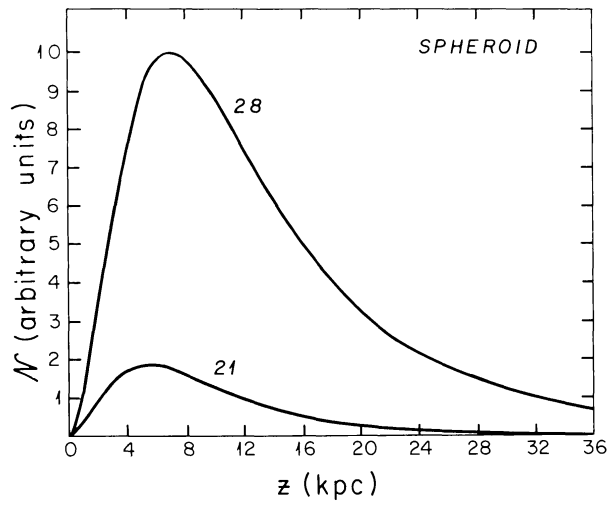

FIG. 7*b*

FIG. 7.—The distribution of visible stars with distance from the Sun. The results are shown for stars in the direction of the galactic pole for both 21st and 28th mag. Separate curves are shown for (*a*) the disk component and (*b*) the spheroidal component. For each component, the area under the curve is proportional to the total number of stars visible to that limiting magnitude. The curves shown were obtained using the standard Galaxy model of Table 1 with zero obscuration.

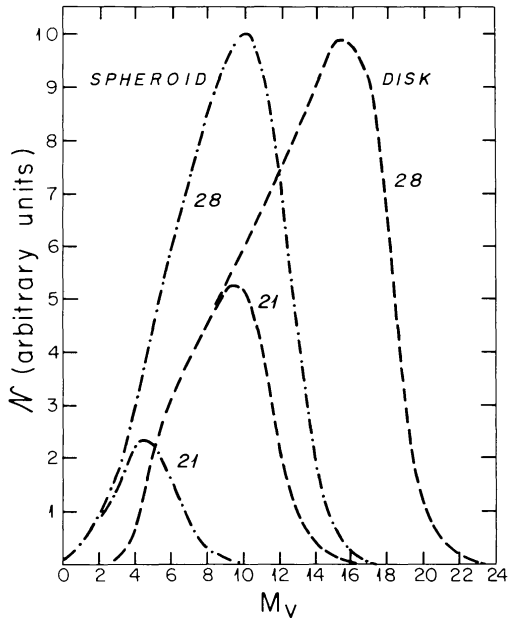

FIG. 8a

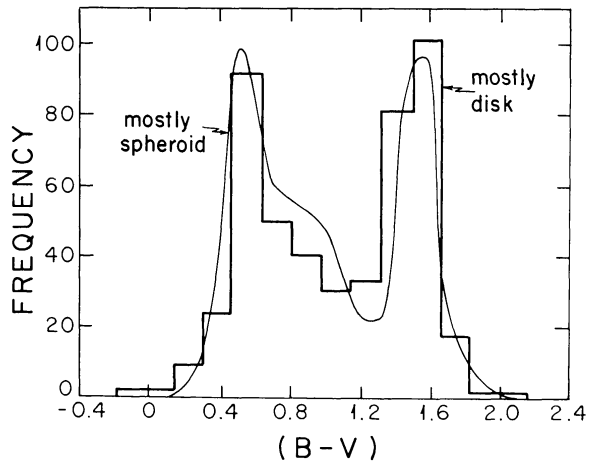

FIG. 8c

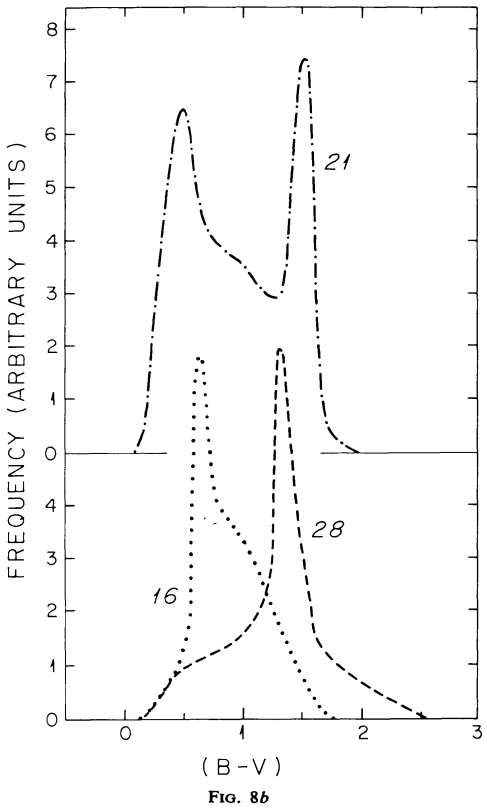

FIG. 8b

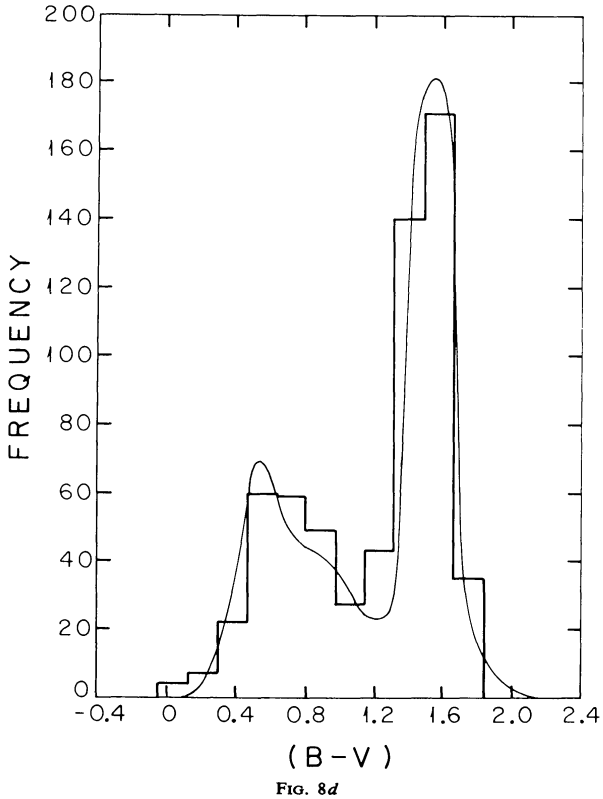

FIG. 8d

FIG. 8.—(*a*) The distribution of visible stars with absolute magnitude for the disk (*dashed lines*) and spheroid (*mixed dots and dashes*) to 21st and 28th mag in the direction of the galactic pole. For each component, the area under the curve is proportional to the total number of stars visible to that limiting magnitude. The curves shown were obtained using the standard Galaxy model of Table 1 with zero obscuration. The relative normalization between components was chosen for convenience in display. (*b*) The predicted distribution of $(B-V)$ colors in the direction of the galactic pole for stars brighter than $m_V=16$, 21, and 28 mag. The curves shown were obtained using the standard Galaxy model of Table 1 with zero obscuration. (*c*) The distribution of $(B-V)$ colors in the direction of the galactic pole for stars with apparent visual magnitudes between 19.75 and 22.0. The curve is the distribution predicted by the standard Galaxy model of Table 1 with zero obscuration. Data from Kron (1978) is plotted as a histogram. (*d*) The distribution of $(B-V)$ colors in the direction of SA 68 ($l=111°$, $b=-46°$) (as in Fig. 8*c*) with A_∞ given by eq. (7).

the model disk counts (Fig. 4*b*) from the available total star count data (see Fig. 4*a*) in order to estimate the spheroid star counts. (The spheroid counts could be obtained directly if the $[B-V]$ colors were measured; see § III*h*.) The best fit to the spheroid counts obtained in this way is $\nu=4.0\pm0.3$ (standard deviation). The principal source of uncertainty in the formal estimate of ν arises from the application of Poisson statistics to the sample of 18 stars used to normalize the local spheroid star density (§ II*b*). The Hubble law, $\nu=3$, is unacceptable at more than the three-sigma level. The above result depends on the local Schmidt normalization for the spheroid. If we ignore the normalization constraint and consider only the rate of increase of the spheroid counts (logarithmic slope) we obtain $\nu=4.0\pm0.5$ (standard deviation). The Hubble law, $\nu=3$, is unacceptable at the two-sigma level. The above results favor the de Vaucouleurs spheroid for which $\nu\approx3.8$. Similar values for ν are found by Spinrad *et al.* (1978) and Kormendy and Bruzual (1978) in NGC 4565, a galaxy thought to be similar to our own.

Detailed numerical calculations show that the star counts are approximately independent of ν for angles that are 40° from the galactic center, assuming that the star density at the solar position is fixed. For large ν, the star density increases faster along the line of sight for $r<r_0$ and decreases faster for $r>r_0$ than for small ν. These opposite trends approximately cancel each other for a line of sight that is about 40° from the galactic center. The best direction for measuring from the star counts the normalization constant C is therefore ($l=0°$, $b=40°$).

In Appendix B we combine generalizations of equations (13a) and (13b) for the disk and spheroid counts separately into a compact formula for the total star counts (both differential and integral).

g) Distributions in Distance and Absolute Magnitude

We examine next the predicted distance distribution (Fig. 7) and the predicted distribution of absolute magnitudes (Fig. 8*a*) for visible stars in the direction of the galactic pole for limiting magnitudes 21 and 28 (calculated assuming $M_d=+\infty$ in eq, [1]). The curves that are displayed were calculated using the standard Galaxy model of Table 1 assuming zero obscuration.

Figure 7 shows how far one sees stars in the Galaxy at 21st and 28th mag (~0.6 kpc for the disk, and ~7 kpc for the spheroid). Visible stars in the spheroidal component are typically an order of magnitude further away than stars in the disk. The decrease in star density with distance from the Sun for both components strongly reduces the scaling of seeing depth, d, with apparent magnitude (for a homogeneous distribution: $d\approx10^{0.2m}$). Between 21 and 28 mag the mean distance of visible stars in the direction of the pole increases by only 10% for the disk and 50% for the spheroid component.

Figure 8*a* shows what parts of the stellar luminosity functions can be studied in magnitude-limited samples. The number of visible disk stars brighter than $M_V=+9$ is essentially the same at 21 and 28 mag. Also, the number of visible spheroid stars brighter than $M_V=+4$ is practically constant between 21 and 28 mag (Fig. 8*a*). Because the sharp density gradient in the disk favors dim stars, the typical visible spheroidal star is ~6 magnitudes more luminous than the typical visible disk star (Fig. 8*a*).

Figure 8*a* also indicates that the ranges measured for both disk and spheroidal luminosity functions (Figs. 1 and 3) include those absolute magnitudes which are expected, on the basis of the standard Galaxy model, to contribute most to the observed number of visible stars to 28 mag. Uncertainties in the luminosity functions outside these intervals may have only a minor effect on the star counts (see, however, § VI on the possible effects of a massive Galaxy halo).

h) Distribution of $(B-V)$ Colors

The predicted distribution of $(B-V)\equiv(m_B-m_V)$ colors for stars in a given apparent magnitude interval $m_1\leq m_V\leq m_2$ can be calculated from the (predicted) distribution of absolute magnitudes (Fig. 8*a*). The transformation from absolute magnitude to $(B-V)$ color is accomplished using the Hertzsprung-Russell diagram. The details of this transformation are presented in Appendix C.

Figure 8*b* is the predicted $(B-V)$ color distribution in the direction of the galactic pole for stars brighter than $m_V=16$, 21, and 28 mag for the standard model (Table 1). The results have been obtained using the data on colors that are summarized in Appendix C. At $m_V=16$ mag the distribution is dominated by relatively blue disk stars with $(B-V)\approx0.75$ and at $m_V=28$ mag by red spheroid stars with $(B-V)\approx1.5$. At $m_V=21$ mag there are two peaks arising from relatively blue spheroid stars with $(B-V)=0.5$ and red disk stars with $(B-V)\approx1.5$.

The double peaked distribution in $(B-V)$ occurs only for a limited range of apparent magnitudes (and directions in the sky, as discussed below). In the region in which the distribution is predicted to be (strongly) double peaked, $18\lesssim m_V\lesssim24$, the two peaks can be used to separate the disk and spheroid stars by their colors alone, e.g., at $m_V=21$ almost all ($\gtrsim85\%$) the stars with $(B-V)\geq1.2$ are from the disk and almost all ($\gtrsim99\%$) the stars with $(B-V)\leq1.2$ are from the spheroid. Note that the disk stars in a magnitude limited sample are significantly *redder* than spheroid stars in spite of the fact that the color distributions for the two components are assumed to be identical in space. (This is a result of the differing density gradients for each component

along the line of sight, § III*g*.) The opposite effect is often assumed, incorrectly, in the literature.

The separation between the disk and spheroid peaks decreases at low galactic latitudes because of the shallower density gradient for the disk along the line of sight. In the direction of the galactic anticenter the spheroid peak is strongly reduced because few stars from that component are seen there.

The double-peak phenomenon is most pronounced in the general direction of the galactic pole for apparent magnitudes $m_V \approx 21$ mag.

We can compare the model color distributions with those measured by Kron (1978) for stars in SA57 ($b = 86°$) near the galactic pole. The data are in the J and F bands with $(B-V) = 0.85\ (J-F)$ according to the color equations in Kron (1978). This relation is probably accurate to ~ 0.05 mag (based on observational comparisons). In Figure 8*c* we compare the model with the data for a range of apparent Visual magnitudes between 19.75 and 22.0. The lower magnitude limit is the maximum brightness considered by Kron; beyond the upper magnitude limit the $(B-V)$ colors are strongly affected by noise in the photometry and by contamination from galaxies. (Between $m_V = 22$ and 24 the mean $B-V$ color becomes bluer by $\frac{1}{2}$ mag. The $B-V$ distributions for stars and galaxies approach each other at these dimmer magnitudes.) The model distribution is calculated for the same sky area as the data, 1080 square arcmin (and has *not* been renormalized to the same total star counts as the data.) The agreement between model and data is excellent and indicates an absence of stars with scale heights intermediate between those of the disk and spheroid. The range of absolute magnitudes corresponding to the gap between the disk and spheroid peaks is $+4 \leq M_V \leq +8$.

The fraction of stars with $(B-V) < 1.2$ is 0.56 in the data and 0.66 in the model. In the model, stars in this color interval come almost exclusively from the spheroid. This result confirms the normalization for the spheroid component calculated in § II*b* based upon the Schmidt (1975) data of high-velocity stars. The Schmidt normalization and the Kron data agree within one sigma, assuming Poisson statistics. (The slight difference in normalization could be due to a magnitude scale difference of ~ 0.15 mag equal to the uncertainty in the obscuration correction at the galactic pole.) In § IV*d* we reexamine the spheroid component normalization for oblate models.

i) Limit on the Quasar Number Density

The agreement between the $(B-V)$ distribution predicted by the model and the Kron (1978) data places a significant constraint on the evolution of QSOs. Bohuski and Weedman (1979) have shown that an extrapolation of the number-magnitude relation for QSOs from $m_V = 19$ mag (where it is reasonably well established) to $m_V = 22$ mag (where it has not previously been determined) predicts that virtually all stellar objects at $m_V = 22$ mag at the galactic pole are QSOs. They stressed that this result implies that number counts of faint stellar objects can provide useful information on quasar evolution. On the other hand, the Kron (1978) data are consistent with nearly all of the stellar objects being galactic (main-sequence) stars.

Most QSOs that have been identified to date are much bluer, $(B-V) \lesssim 0.40$, than faint disk or spheroid stars (white dwarf stars are discussed below). In the catalog of (primarily) radio identified QSOs compiled by Burbidge, Crowne, and Smith (1977), about 60% of the objects have $(B-V) \leq 0.30$. Only 2% of the stellar objects with $19.95 \leq (m_J + m_F)/2 \leq 22.15$ or about $20.0 \leq m_V \leq 22.2$ in the Kron (1978) data have $(J-F) \leq 0.35$. The value of $(J-F) = 0.35$ corresponds to $(B-V) = 0.30$ for both stars and QSOs for a variety of spectral distributions. Assuming that 60% of the QSOs with $m_V \leq 22$ have $(B-V) \leq 0.30$, then the number of QSOs brighter than $m_V = 22$ mag must be $\lesssim 65$ deg^{-2} (unless the average QSO colors become much redder at faint magnitudes; see e.g., Bahcall and Sargent 1967). This estimate is an upper limit for the QSO surface because most white dwarf stars also have $(B-V) \leq 0.30$. The standard model predicts (based on the fraction of all stars that are white dwarfs as given by eq. [18], below) that the number density of white dwarf stars that have $(B-V) \leq 0.30$ (i.e., $M_V \leq 13.0$, [Sion and Liebert 1977]) in the above apparent magnitude range $20.0 \leq m_V \leq 22.2$ is 10 deg^{-2}. Hence the number of QSOs brighter than $m_V = 22$ mag ($m_B = 22.5$ mag) is $\lesssim 50$ deg^{-2}. This is between one and two orders of magnitude smaller than the number density predicted by the extrapolation of the observed number-magnitude relation for QSOs between $m_V \approx 16$ to $m_V \approx 20$ (Steppe, Veron, and Veron 1979; Bohuski and Weedman 1979; Schmidt 1978; Wills 1978; Osmer 1978; Braccesi *et al.* 1980). Our constraint on the density of QSOs is not much larger than the number density of confirmed QSOs (~ 13 deg^{-2}, from an incomplete list to $m_B = 21$) in the sample of Hoag and Smith (1977).

Proper motion studies of stellar objects permit a *color-independent* check on these results since QSOs appear as stationary objects in these surveys. Some Galactic stars will also appear to be stationary because the combination of their peculiar velocity and distance from the Sun results in an angular motion below the threshold of detection. Chiu (1980) has obtained proper motions in a small (0.09 square degree) field in SA57 near the galactic pole. His survey is said to be complete to $m_V = 20.5$ but appears to be complete to the tabulated limit of $m_V = 21.25$. In the Chiu sample, there are six stellar objects that appear to be stationary (a proper motion less than the uncertainty in the proper motion) corresponding to 66 deg^{-2}. A simple velocity disper-

sion model applied to our standard Galaxy model indicates that many of these objects ($\gtrsim$50%) are galactic stars. Over the magnitude range the Kron (1978) and Chiu (1980) data have in common, $20.0 \leq m_v \leq 21.25$, the number of QSOs inferred from the Chiu proper motion sample is $\lesssim 40 \pm 20$ deg^{-2} (corrected for galactic stars and statistically corrected for 32% of the stationary objects which have measured proper motions greater than their estimated errors) and from the Kron sample is $\lesssim 30 \pm 11$ deg^{-2} (corrected for white dwarf stars, as above).

IV. UNCERTAINTIES IN THE LUMINOSITY FUNCTIONS AND SPATIAL DISTRIBUTIONS

We will discuss in § IV*a* and IV*b* the sensitivity of the predicted counts in the direction of the galactic pole to the uncertainties in the luminosity functions, ϕ, and the parameters that specify the density functions, ρ. In § IV*c* we consider constraints on the model parameters imposed by the variation of the star counts with latitude and longitude. In § IV*d* we consider the effects of an oblate spheroidal component on the star counts. Finally, we discuss in § IV*e* the effects of a possible "hole" in the star distribution near the galactic center. (Throughout this section we use the standard Galaxy model of Table 1.)

a) Uncertainties in the Luminosity Functions

The behavior of the luminosity functions is uncertain at the bright and dim ends. At the bright end the function may fall off faster than a power law and reach an effective maximum luminosity. At the dim end, the disk function ceases to increase and there is some evidence that it may decrease (Luyten 1968). We simulate these effects by varying the bright end cutoff, M_b, and the dim end cutoff, M_d, of the luminosity function beyond which $\phi \equiv 0$ (eq. [1]). For the disk, we find that the counts for all apparent magnitudes ≤ 28 change by no more than $\pm 10\%$ when M_d for the disk varies between +18th and +28th mag; the total counts (disk plus spheroid) do not change by more than $\pm 2\%$. There is little change ($\lesssim 1\%$) in the counts for $m > 10$ when M_b is varied from +3 to −10. The luminosity function for the spheroidal component has been measured over the restricted (Visual) range of about +4 to +12. For the spheroid, the counts for all apparent magnitudes ≤ 28 change by no more than $\pm 7\%$ when M_d for the spheroid varies between +13 and +28. The spheroid counts change by $\lesssim \pm 10$ percent for $m > 10$ when M_b is varied from +3 to −10; the total counts (disk plus spheroid) do not change by more than $\pm 5\%$. We conclude that the star counts to 28 mag in the Visible band are not significantly affected by uncertainties considered in the bright and dim ends of the disk and spheroidal luminosity functions.

The luminosity functions may increase drastically outside the available data limits. The modifications considered above all assume a luminosity function with the analytic form given in equation (1). Consider a luminosity function $\phi(M) \propto 10^{\sigma M}$. Then the number density $\mathcal{N}(\leq m) \sim 10^{\sigma m}$ from equation (5). Hence the asymptotic form of $\mathcal{N}(\leq m)$ for dim apparent magnitudes is the same as the asymptotic form of ϕ. The knee in the disk counts above $m = 16$ (Fig. 4) arises from the exponential fall in density with height above the plane together with a general flattening of the luminosity function at the dim end (Fig. 1). This knee will be diminished or even disappear for a sufficiently steep rise in the luminosity function (of logarithmic slope σ) beginning at some absolute magnitude, M_e. Define the fractional increase in counts, $\Delta\mathcal{N}/\mathcal{N}$, resulting from a change in the luminosity function as

$$\Delta\mathcal{N}/\mathcal{N} = \frac{\mathcal{N}_{M_e,\sigma}(\leq m) - \mathcal{N}(\leq m)}{\mathcal{N}(\leq m)}, \qquad (14)$$

where $\mathcal{N}(\leq m)$ is the standard model counts. We assume that the luminosity function is continuous at $M = M_e$ and increases like $10^{\sigma M}$ for $M \geq M_e$. We have computed, for illustrative purposes, $\Delta\mathcal{N}/\mathcal{N}$ at $m_V = 28$ mag for a not unreasonable value of $\sigma = 0.2$ and a rather extreme value of $\sigma = 0.4$. (Note for comparison that the luminosity function in Fig. 1 has a slope of ~ 0.6 from $M_V = -6$ to 0 and a slope of ~ 0.1 from $M_V = +2$ to +8.) We find that with $\sigma = 0.2$ the change in disk counts $(\Delta\mathcal{N}/\mathcal{N})_{\rm disk}$ varies from 0.9 for $M_e = +16$ to 0.1 for $M_e = +20$, while for $\sigma = 0.4$ $(\Delta\mathcal{N}/\mathcal{N})_{\rm disk}$ is 8 at $M_e = +16$ and 0.2 at $M_e = +20$. The corresponding fractional changes in the *total* counts are about a factor of 5 smaller than the above-quoted changes in disk counts. The choice of $M_e = +16$ corresponds to a rise in the luminosity function just where the data end. The increase in counts to 21st mag is negligible. The knee in the counts of disk stars disappears for $M_e = +16$, $\sigma = 0.4$. Moreover, the number of disk stars is much greater than the number of spheroid stars at $m = 28$. Nevertheless, for plausible parameter choices the total star counts are not drastically changed, although differences of a factor of 2 are possible (and could be detected with the Space Telescope). (Luyten has obtained a luminosity function to $M \approx +24$ that decreases dimward of $M \approx +16$. There is a significant uncertainty in this result which has not yet been confirmed by other observers.)

For the spheroid, the increase in star counts to 28th mag with M_e chosen to be +12 (the data limit) is +10% for $\sigma = 0.2$ and +60% for $\sigma = 0.4$. For $M_e = +16$, the change in the counts is $\lesssim 1\%$ for $\sigma \leq 0.4$. We conclude that observable effects ($\geq 20\%$ increase in total counts) are possible if the luminosity functions $\phi \sim 10^{\sigma M}$ for $M \geq M_e$ with $\sigma \gtrsim 0.2$ and $M_e \lesssim +16$ mag.

b) Variations in Density Distributions

Variations in the spatial distributions of each component affect the model counts by calculable amounts. The bright end of the disk luminosity function contributes little to the star counts primarily because the scale heights for these stars are small. Hence the counts should be practically independent of the uncertainties in the spatial distribution of such stars. If the exponential scale height for the brightest disk stars, ($M \lesssim +3$) is varied from 70 to 110 pc (Fig. 2) there is $\lesssim \pm 1\%$ change in both the disk and total counts for $m_V > 10$. If the exponential scale height for the dimmer stars ($M \gtrsim +5$) is varied from 275 to 375 pc, there is a $\pm 50\%$ change in the disk counts, but the total counts (disk plus spheroid) do not change by more than $\pm 15\%$ for all apparent magnitudes ≤ 28.

For the spheroid, a change in the distance of the Sun from the center of the Galaxy from 7 kpc to 9 kpc changes the counts by $\lesssim \pm 25\%$ for all $m \leq 28$.

c) Constraints Due to Count Variations with Latitude and Longitude

We calculate variations in the star counts caused by changing by large amounts the most important parameters that define the standard Galaxy model (Table 1). We are thus able to determine the sensitivity (and reliability) of the predicted model counts and to indicate the most useful regions in which to acquire further data.

In Table 3, we indicate the change in the star counts, $\mathcal{N}'/\mathcal{N}_0$, for variations in the distance of the Sun from the galactic center, r_0; in the scale length of the disk in the plane, h, (eq. [2c]); and in the characteristic distance of the spheroid, r_e (eq. [4]). $\mathcal{N}_0$ is the integrated star density for the standard Galaxy model (Table 1 with obscuration $A = 0$). The value $\mathcal{N}'$ is the star density for the parameter value indicated in the table. $\mathcal{N}'/\mathcal{N}_0$ is given for 12, 18, and 28 mag at the galactic pole and at latitude 20° for longitudes 0°, 90° and 270°, and 180° (the calculated results are virtually identical for a cosecant obscuration law and for one with no obscuration, i.e., $A = 0$). Table 3 shows that the change in the counts with longitude is typically about as large as with latitude for the parameter variations considered.

The length parameters are as follows: the distance of the Sun from the galactic center ($r_0 = 7$ kpc–9 kpc), scale length of the disk in the plane ($h = 2.5$ kpc–4.5 kpc), and characteristic distance of the spheroid ($r_e = 2.25$ kpc–3.0 kpc). These do not greatly affect the predicted model star counts. Detailed information on the spheroidal component can be obtained by measuring the star counts and colors at selected latitudes and longitudes at moderate to faint magnitudes, 18 mag$\lesssim m_V \lesssim$28 mag.

d) Oblate Models

We investigate next oblate models in which the spheroid star distribution has a smaller characteristic scale length in the direction (z) perpendicular to the galactic disk than it does in the plane of the disk (x).

The distribution of globular clusters in the Galaxy suggests an axial ratio more nearly equal to unity (Harris 1976; de Vaucouleurs and Buta 1978), although infrared measurements at very low latitudes ($b < 7°$) near the center of the Galaxy are consistent with a nonzero ellipticity (see Maihara *et al.* 1978).

The transformation $z' = \kappa z$ changes the spheroid into an ellipsoid of revolution with axis ratio κ and ellipticity $\varepsilon = (1 - \kappa)$. The characteristic radii for the spheroid in the x and z directions become $r_e{}^x$ and $r_e{}^z$, respectively. We set $r_e{}^x r_e{}^z = r_e{}^2 = (2.67 \text{ kpc})^2$. The variation of the star counts with r_e was demonstrated to be small in § IV*c* and Table 3.

The star count data together with the Schmidt (1975) normalization for the local spheroid star density constrain strongly the allowed axis ratio. In order to calculate the probable range of ellipticities ε allowed by the data, we must estimate the observational uncertainty in the star counts and in the Schmidt normalization (§ II*b*). The average of the star counts at 21 mag from the

TABLE 3

VARIATION IN THE STAR COUNTS WITH LATITUDE AND LONGITUDE AS A FUNCTION OF MODEL PARAMETERS[a]

Latitude and	$\mathcal{N}'/\mathcal{N}_{\text{standard}}$											
	$b^{II} = 90°$			$b^{II} = 20°, l^{II} = 0°$			$b^{II} = 20°, l^{II} = 90°$			$b^{II} = 20°, l^{II} = 180°$		
Longitude	m12	18	28	12	18	28	12	18	28	12	18	28
$r_0 = 7$ kpc.....	0.99	0.94	0.81	0.99	0.87	0.76	1.00	0.98	0.95	1.00	1.00	0.98
$r_0 = 9$ kpc.....	1.00	1.06	1.22	1.00	1.15	1.30	1.00	1.02	1.06	1.00	1.00	1.02
$h = 2.5$ kpc	1.00	1.00	1.00	1.04	1.10	1.15	1.00	0.98	0.96	0.96	0.86	0.82
$h = 4.5$ kpc	1.00	1.00	1.00	0.98	0.96	0.95	1.00	1.01	1.02	1.02	1.07	1.10
$r_e = 2.25$ kpc ...	1.00	0.99	0.94	1.02	1.05	1.05	1.00	1.00	0.99	1.00	1.00	0.99
$r_e = 3.0$ kpc	1.00	1.01	1.05	0.99	0.97	0.97	1.00	1.00	1.01	1.00	1.00	1.01

[a] Standard model (Table 1); star density in stars degree^{-2} brighter than magnitude m. The tabulated quantity is $\mathcal{N}'/\mathcal{N}_{\text{standard}}$, where $\mathcal{N}_{\text{standard}}$ is the star density for the standard model (Table 1 with $A = 0$) and $\mathcal{N}'$ is the star density with the parameter value indicated.

three sources of data in the V band (§ IIIb), above) is 705 stars mag^{-1} degree^{-2}, with a standard deviation of 110 counts. We use Poisson statistics to estimate the uncertainty in the normalization derived from Schmidt's sample of 18 stars.

The spheroid star counts predicted by the model in the direction of the galactic pole at $m_V=21$ mag, $\mathcal{N}_s(b=90°)$, are reduced from the values found for $\varepsilon=0$ by factors of 1.9 for $\varepsilon=0.25$ and 4.6 for $\varepsilon=0.5$. The total star counts, $\mathcal{N}_T$, are reduced from the values found for $\varepsilon=0$ by factors of 1.5 and 2.25, respectively. These reductions are due to the greater density gradient in the direction of the pole when $\varepsilon \geq 0$. The model (with Schmidt normalization) that matches the star count data at $m_V=21$ has $\varepsilon=0.05\pm0.15$. The uncertainty in ε reflects the scatter in the star count data and the expected statistical noise in the Schmidt normalization.

If we allow the possibility that the Schmidt normalization could be subject to nonstatistical errors and hence need not necessarily constrain the permitted ellipticities for the Galaxy, then we are free to renormalize each of the ellipsoidal models so that the predicted star density matches the observations at $m_V=21$ at the galactic pole. The ellipticity ε must then be determined from the variation in the counts with latitude and longitude or from the $(B-V)$ color distribution of visible stars away from the pole. The $\mathcal{N}(m)$ relation for $\varepsilon=0$, which is averaged over longitude, shown in Figure 4a is only slightly affected for models with $\varepsilon \leq 0.50$ after renormalization. For $\varepsilon=0.5$, the maximum deviation from the $\varepsilon=0$ relation is ~20% for latitudes b between 20° and 90°, which is probably of the same order as the observational uncertainties in the existing data.

We specify in what follows those directions that will be most useful in determining the ellipticity without relying upon the Schmidt normalization of the local spheroid star density. Directions in the $l=(0°,180°)$ plane suffer the least from interference by disk stars. The greatest variation of spheroid counts occurs in the direction of the anti-center (at $b=20°$, $l=180°$, the variation between $\varepsilon=0$ and 0.25 is 2:1); however, the disk counts in this direction are a factor of 10 greater than the spheroid counts. (The least variation with ε is at $b=90°$, by definition, since we choose to normalize the model counts for nonzero ellipticity to agree with observations at the pole, and at $b=20°$, $l=0°$.) In the direction of the galactic center, the greatest variation with ε is at $b=40°$ where the spheroid counts for $\varepsilon=0.25$ and $\varepsilon=0.5$ are reduced from their values for $\varepsilon=0$ by 14% and 32%, respectively, at $m_V=21$. The disk counts comprise only one-fifth of the total counts at $l=0°$, $b=40°$. In the direction of the anti-center, the best compromise is at $b=60°$; in this direction the spheroid counts for $\varepsilon=0.25$ and $\varepsilon=0.5$ increase from their values at $\varepsilon=0$ by 32% and 70%, respectively, at $m_V=21$ mag. The disk counts, however, comprise one-half of the total counts at $l=180°$, $b=60°$. Data in these two directions ($l=0°$, $b=40°$ and $l=180°$, $b=60°$) are not presently available.

The $l=(90°,270°)$ plane defines another important set of directions. The spheroid counts in this plane are independent of latitude for $\varepsilon=0$. Measurements at two or more latitudes of the star counts in this plane would form an important test of the hypothesis that $\varepsilon=0$ for the spheroid. Contamination from the disk, however, can be large in this plane (e.g., at $l=90°$, $b=30°$; the disk to spheroid star density ratio at $m_V=21$ mag is 2.5:1, a factor of 6 greater than at the pole.

The separation in $(B-V)$ colors between stars in the disk and spheroid (Figs. 8b and 8c) for $m_V=21$ can be used to minimize the effects of this disk contamination. Kron (1978) has obtained star counts and $(J-F)$ colors in SA 68 ($l=111°$, $b=-46°$), which is reasonably close to the desired $l=90°$ direction. The $(B-V)$ colors for stars with apparent magnitudes m_V between 19.75 and 22.0 (see § IIIh) are plotted in Figure 8d together with the predicted distribution for the standard model with $\varepsilon=0$. (See § IIIh for the equation relating $B-V$ and $J-F$). The model distribution was calculated for the same sky area as the data, 1075 square arcmin (and has *not* been renormalized to the same total star counts as the data). The centroid of the spheroid peak in the $(B-V)$ diagram is somewhat dependent on ε. For $\varepsilon=0.5$ it is shifted by about +0.15 mag redward (both at the pole and in SA 68) with respect to the distribution for $\varepsilon=0$, as a result of the sharper density gradient. The agreement is good. However, the number of (primarily spheroid, ~99%) stars with $(B-V)\leq 1.1$ in the model with $\varepsilon=0$ is slightly smaller (~5%) than in the data. In the direction of the galactic pole the number of (primarily spheroid) stars with $(B-V)\leq 1.1$ in the model with $\varepsilon=0$ is somewhat larger (~30%) than in the data (§ IIIh, Fig. 8c). A difference in the magnitude calibration of order ±0.1 mag for each field could be responsible for the effect.

Another possible explanation for the above-mentioned discrepancy is that the spheroidal component is not perfectly spherical. There are 248 stars in SA 57 ($b=86°$, very close to the galactic pole) and 228 in SA 68 with $(B-V)\leq 1.1$. In order to estimate the ellipticity implied by the observations, we normalize the model to give 248 stars with $(B-V)\leq 1.1$ in the direction of SA 57 and then find the ellipticity that yields 228 stars with $(B-V)\leq 1.1$ in the direction of SA 68. We obtain $\varepsilon=0.15\pm0.07$ for both a Sandage obscuration model (eq. [7]) and a cosecant obscuration model (eq. [6]). For a model with $\varepsilon=0.15$, the Schmidt normalization for the local spheroid star density must be increased by 12% (§ IIb), which is less than the uncertainty estimated from Poisson statistics applied to the Schmidt (1975) data sample. The total (disk plus

spheroid) star counts predicted by a model with $\varepsilon=0.15$ and normalized to the Kron data are similar to those for the standard spherical model with $\varepsilon=0$. The differences between models ($\lesssim 15\%$) are comparable to the uncertainties in the data. The differences increase for dimmer magnitudes. At $m_V=30$ the difference between models is $\lesssim 25\%$ (with the larger errors occurring at medium latitudes, $\sim 50°$, near longitude zero).

The above discussion refers only to the de Vaucouleurs density function for the spheroid. In § III*f* we showed that the de Vaucouleurs relation was strongly favored over the Hubble form in the spheroidal case, $\varepsilon=0$. Since the ellipticity, ε, and the index, ν, of the power-law density function (§ III*f*) are coupled, it is necessary to reexamine the Hubble law, $\nu=3$, for nonzero ellipticities. There are two parameters, the local spheroid density normalization and the ellipticity ε. In considering the Hubble law, we use again the following facts (from the Kron data sample): 248 stars in SA 57 and 228 stars in SA 68 have $(B-V)\leq 1.1$ and $19.75\leq m_V\leq 22.0$. Setting the local normalization for the spheroid equal to the Schmidt value (§ II*b*), we obtain an ellipticity of $\varepsilon=0.32$ by matching the model star counts (with the Hubble law) to the Kron data in SA 57. For $\varepsilon=0.32$, the model counts in SA 68 are 20% larger than in SA 57, instead of 10% smaller (as in the Kron data sample). If we include the statistical uncertainty of the Schmidt normalization, this discrepancy is two standard deviations. Letting the local normalization be a free parameter, one can uniquely solve for both ε and the normalization using the Kron data. We obtain $\varepsilon=0.15$ and a local spheroid normalization that is smaller than the Schmidt value by a factor of 1.7—a three-sigma discrepancy for the normalization, assuming Poisson statistics. We can reinforce this result by examining the variation of $\mathscr{A}$ with apparent magnitude as in § III*f*, but for a Hubble law with ellipticity $\varepsilon=0.15$. With the Schmidt normalization, the Hubble law is unacceptable at more than the three-sigma level of significance. Ignoring the normalization constraint and considering only the rate of increase of the spheroid counts, the Hubble law is still unacceptable by 2 standard deviations.

In summary, the Hubble law disagrees with observations at about the two-sigma or three-sigma level of significance, depending on precisely what is assumed.

Star counts obtained with ground-based telescopes could yield a much more accurate determination of ε. Accurate $(B-V)$ colors to $m_V\approx 21$ mag for several widely spaced fields in the selected directions noted above ($l=0°, b=40°$ and several values of b in the $l=90°$ to 270° plane) are required. The fields should have fairly large areas ($\gtrsim 1$ degree^2) in order to reduce the importance of uncertainties arising from Poisson statistics. Because there is no improvement in the sensitivity to ε from $m_V=21$ mag to $m_V=28$ mag, observations obtained with ground-based telescopes will be important and sufficient.

e) Star Density Near the Galactic Center

We consider next the possibility that the disk population may have a stellar "hole" near the galactic center. Following Kormendy (1977*a*), we assume for illustrative purposes a perturbed density of stars in the disk, ρ_d', of the form

$$\rho_d'=\rho_d\begin{cases}\exp\left[-(r_c/x)^3+(r_c/r_0)^3\right], & x\leq r_0;\\ 1, & x>r_0.\end{cases} \tag{15}$$

Here ρ_d is the unperturbed density of disk stars (eq. [2b]) and r_c is some cutoff radius interior to which the star density falls off rapidly. We have recomputed the integrated star counts at a variety of latitudes ($b\geq 20°$), longitudes and cutoff radii using equation (15) for the disk density and the standard de Vaucouleurs form for the spheroid density. For $r_c=3$ kpc, i.e., an assumed stellar "hole" in the inner 3 kpc of the Galaxy, the maximum change in the integrated counts is only 8% (at $m_V=28$ and $l=0°, b=20°$). Even if r_c is as large as 5 kpc, the maximum decrease in the integrated counts is only 15% for $b\geq 20°$. We conclude that the observable star counts are insensitive to characteristics of the disk near the center of the Galaxy. (This result can also be inferred in a less formal way from Fig. 7*a*.)

V. SOME CHARACTERISTICS OF THE STANDARD GALAXY MODEL

The principal characteristics of the standard Galaxy model are defined by the disk and spheroid components derived in § II. We calculate and discuss in this section some of the galactic parameters implied by this model including local and total mass and luminosity densities, mass-to-light ratios for each of the components, Oort constants, number of stars, escape velocity, and angular momentum of the disk.

a) Stellar Densities and Distributions

i) *Local Stellar Quantities*

The luminosity density, $\mathscr{L}_L$, the visible stellar mass density $\mathscr{L}_{\mathscr{M}}$, and the star number density, $\mathscr{L}_N$, can be computed for the Solar neighborhood using the luminosity functions ϕ (see eq. [1]) for the disk and spheroidal components that were discussed in § II*a* and II*b*. One has:

$$\mathscr{L}_L=\int_{-\infty}^{+\infty}10^{-(M-M_\odot)/2.5}\phi(M)\,dM,\quad (L_\odot/\mathrm{pc}^{-3}),$$

$$\mathscr{L}_{\mathscr{M}}=\sum_i\int_{-\infty}^{\infty}\mathscr{M}_i(M)f_i(M)\phi(M)\,dM,\quad (\mathscr{M}_\odot/\mathrm{pc}^{-3}),$$

$$\mathscr{L}_N=\int_{-\infty}^{\infty}\phi(M)\,dM,\quad (\text{stars pc}^{-3}), \tag{16}$$

where the solar luminosity in the Visual band is $M_\odot = +4.83$. $\mathcal{M}_i(M)$ is the mass-luminosity relation in the Visual band for stars of luminosity class i (e.g. supergiants, main-sequence stars, white dwarfs, *etc.*) and $f_i(M)$ is the fraction of stars with absolute magnitude M for luminosity class, i. In practice, only main-sequence stars and white dwarfs need be considered, as they contain virtually all of the visible mass (see below). We use the following mass-luminosity relation for main-sequence stars, $i = \mathrm{MS}$:

$$\log \mathcal{M}_{\mathrm{MS}} = -0.09280\, M_V + 0.448, \quad M_V \geq 0,$$

$$\log \mathcal{M}_{\mathrm{MS}} = -0.2710\, M_V + 0.448, \quad M_V \leq 0, \quad (17)$$

which accurately fits the data for the approximately 100 binary stars (which have a range in M_V from +4 to +17) listed by Harris, Strand, and Worley (1963).

The fraction of observed stars that are white dwarfs can be calculated using the white dwarf luminosity function derived by Sion and Liebert (1977) for $M_V \leq +15$ and Liebert *et al.* (1979) for $M_V > +15$, in conjunction with the total luminosity function, ϕ (eq. [1]). The number of white dwarfs in the solar neighborhood can be estimated from the above references to be 0.008 pc^{-3}. The corresponding local white dwarf mass density is $0.005\, \mathcal{M}_\odot\ \mathrm{pc}^{-3}$ for an assumed luminosity-independent mass of $0.65\, \mathcal{M}_\odot$. This mass density is smaller than some authors have indicated previously because we have used the results of Liebert *et al.* (1979), which suggest that the white dwarf luminosity function decreases rapidly beyond $M_V = +15$. The fraction of stars on the main sequence is given approximately by

$$f_{\mathrm{MS}}(M_V) = 1 - 0.15 \times 10^{-0.25|M_V - 15|}. \quad (18)$$

The densities for the solar neighborhood computed using equations (16)–(18) have been summarized in Table 4 for the disk (col. [2]), the spheroid (col. [3]), and their sum (col. [4]). The mass density for main-sequence stars increases by less than 10% when the dim end cutoff of the luminosity function M_d is changed from +19 to $+\infty$ (assuming that the luminosity function remains flat for $M \geq 15$ and applying the mass-luminosity relation of eq. [17]).

Figure 9 shows, as a function of main-sequence absolute magnitude, the relative contribution to the luminosity density and to the mass density of the disk (in the plane only) and the spheroid. The main stellar contributors to the luminosity density are different from the main contributors to the mass density. The relative contribution of stars of different absolute magnitudes to the star counts for dim apparent magnitudes ($m_V \geq 21$, shown in Fig. 8*a*) is similar to the mass-density distribution in Figure 9. The density functions (eqs. [2*b*] and [3]) in other galaxies are determined by measuring the luminosity profiles, and hence they indicate the distribution of bright stars. The results of this paper demonstrate that these same density functions describe the distribution of the significantly dimmer stars that dominate the star counts in our galaxy.

ii) *Total Stellar Quantities*

Values of the total luminosity, visible stellar mass, and number of stars can be calculated from relations

TABLE 4

SOME COMPUTED PROPERTIES OF THE STANDARD TWO-COMPONENT GALAXY[a]

	Disk	Spheroid	Disk + Spheroid
Solar Neighborhood			
Luminosity density ($L_\odot\ \mathrm{pc}^{-3}$)	0.062	7.7(−5)	0.062
Mass density of main sequence stars $\mathcal{M}_\odot\ \mathrm{pc}^{-3}$	0.040	5.0(−5)	0.040
Mass density of white dwarfs stars	0.005	6.3(−6)	0.005
Star number density (stars pc^{-3}) for stars $M_V \leq +19$	0.15	1.9(−4)	0.15
Total			
Luminosity ($L_\odot$)	1.2(+10)	1.9(+9)	1.4(+10)
Mass of visible stars ($\mathcal{M}_\odot$)	2.0(+10)	1.4(+9)	2.2(+10)
Mass ($\mathcal{M}_\odot$)[b]	5.6(+10)	3.3(+9)	6.0(+10)
Mass enclosed within r_0 ($\mathcal{M}_\odot$)[b]	3.7(+10)	2.4(+9)	4.0(+10)
Number of stars ($M_V \leq +19$)	7.2(+10)	4.6(+9)	7.6(+10)
Absolute Visual magnitude (no obscuration)	−20.4	−18.4	−20.5
Radius enclosing 90% mass (kpc)	13	19	13
Escape velocity from galactic center ($\mathrm{km\ s}^{-1}$)	385	165	420
Escape velocity from the Sun ($\mathrm{km\ s}^{-1}$)	255	55	260
Angular momentum ($\mathcal{M}_\odot\ \mathrm{kpc}^2\ \mathrm{s}^{-1}$)	1.9(+3)	0	1.9(+3)

[a] See Table 1 for a summary of the model.

[b] Local mass density of $0.15\, \mathcal{M}_\odot\ \mathrm{pc}^{-3}$ assumed. Interstellar matter of local density $0.045\, \mathcal{M}_\odot\ \mathrm{pc}^{-3}$ is assumed to be distributed like the visible stars in the disk but with a scale height of 125 pc. Remaining (dark) matter is assumed to be distributed like the visible stars in both disk and spheroid.

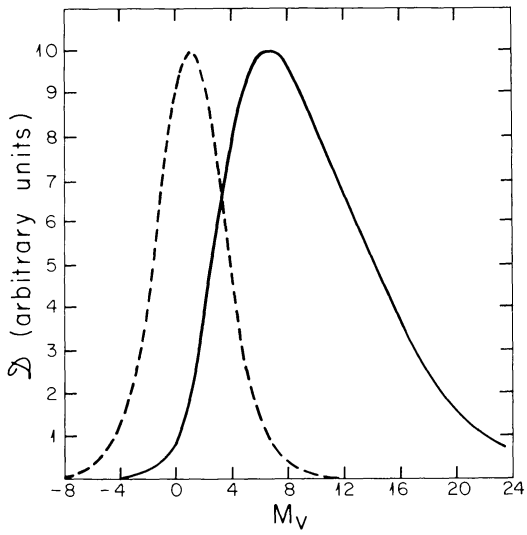

FIG. 9.—The relative stellar contribution of the disk (in the plane only) and the spheroid as a function of absolute magnitude (assuming $M_d = +\infty$) to the luminosity density (*dashed line*) and to the mass density (*solid line*).

that are similar to equation (16), but which include the variation in density ρ with position (eqs. [2c] and [4]). Integrating over all space, one has

$$T_F = \int F(M)\rho(\mathbf{r}, M)\, dM\, dv, \qquad (19)$$

where T_F is the total value for the quantity F and dv is the volume element. For the disk, it is convenient to perform the z integration first and consider surface (or column) densities σ.

The surface densities of the disk for luminosity, σ_L, visible stellar mass, $\sigma_{\mathcal{M}}$, and star number, σ_N, at the solar position, r_0, are, respectively, 16.0 $L_\odot$ pc^{-2}, 27.0 $\mathcal{M}_\odot$ pc^{-2}, and 95 stars brighter than $M_V = +19$ pc^{-2}. The integral of any surface density σ_F over the disk is $2\pi h^2 \sigma_F(r_0)\exp(r_0/h)$, which is sensitive to h, the scale length of the disk in the plane.

Values of the total stellar luminosity, mass in visible stars, and number of stars with $M_V \leq +19$ are listed in Table 4 for the disk, the spheroid, and their sum. Also listed is the total Visual magnitude without obscuration, -20.5 mag. This value compares favorably with the mean value for Sbc galaxies of -20.3 ± 1.0 (Visual) in the *Reference Catalogue of Bright Galaxies* (de Vaucouleurs, de Vaucouleurs, and Corwin 1976) assuming a Hubble constant of 100 km s^{-1} Mpc^{-1}. For a Hubble constant of 50 km s^{-1} Mpc^{-1}, the model Galaxy is 1.5 standard deviations dimmer than the mean. Note that the sample in the *Reference Catalogue* is approximately equivalent to a magnitude-limited sample and therefore is biased in favor of bright galaxies. Hence, the model Galaxy is typical of the brighter Sbc galaxies for Hubble constants in the range of 50–100 km s^{-1} Mpc^{-1}.

The ratio of disk to spheroid luminosities is 6, in agreement with the proposed Sbc type for the Galaxy (van den Bergh 1976). Our value for the disk luminosity is about equal to the estimate of de Vaucouleurs and Pence (1978). Our value for the spheroid is about 1 mag dimmer than theirs. The de Vaucouleurs and Pence determination of the spheroid luminosity was obtained by integrating photometrically the surface brightness in star fields that contained no stars brighter than $m_V \approx 15$, in order to try to subtract the disk component, which contributes $\sim$20 times more to the total surface luminosity density than the spheroid component. This method is subject to a number of uncertainties. For example, the selection of "empty" star fields might lead to unknown biases. The subtraction of two large surface luminosity densities in order to estimate the small spheroid contribution leads to appreciable statistical errors, and could cause a systematic error if the disk contribution is inaccurately modeled. De Vaucouleurs and Pence assumed that the fraction of the disk surface brightness contributed by stars fainter than 15 mag was independent of latitude and equal to the fraction measured at the galactic pole. In our standard model, the fraction of the disk surface brightness contributed by stars fainter than 15 mag increases from 4% at the galactic pole to 18% at a latitude of 20°. The star counts used in the present study are an independent and perhaps more reliable estimator for the spheroid component.

b) Total Masses and M/L Values

The local mass density inferred from star motions out of the plane is 0.15 $\mathcal{M}_\odot$ pc^{-3} (Oort 1960). Of that, 0.045 $\mathcal{M}_\odot$ pc^{-3} is contributed by visible stellar mass (Table 4) and 0.045 $\mathcal{M}_\odot$ pc^{-3} by interstellar matter (Spitzer 1978). The remaining "missing" (dark) matter is 0.06 $\mathcal{M}_\odot$ pc^{-3}. The interstellar matter has the same scale length in the plane as the stellar disk component (§ II*a*), and a scale height of 125 pc (Spitzer 1978), assumed to be independent of distance from the galactic center. We assume in this section (but *cf.* § VI) that the mass density of "missing" matter is everywhere proportional to the visible mass density in both the disk and spheroid. The local ratio of (missing plus visible mass)/(visible mass) is then 2.3 for the disk and spheroid. These values enable us to derive the estimates for the total mass and the mass enclosed within the solar distance r_0 that are given in Table 4 for the disk and spheroid.

No more than 5% of the local total mass density (including dark matter) can be associated with a spherical, spheroidal component. If 5% of the total local mass is in the spheroid, the mass enclosed within the solar position would increase by a factor of order 4 above

that in our standard model (and the solar rotational velocity in the Galaxy would rise to unacceptable values $\gtrsim 350$ km s^{-1}; see below). For an oblate spheroid with ellipticity $\epsilon \lesssim 0.5$ (§ IV*d*), the fraction of the mass density associated with the spheroid is then $\lesssim 10\%$. This suggests that *most of the dark matter is associated with the disk component.*

The mass-to-light ratio, (M/L), for the disk is 5 solar units (Visual), about equal to the mean found by Roberts (1975) for about 80 spiral galaxies for a Hubble constant of 100 km s^{-1} Mpc^{-1}. However, the dispersion about the mean is almost as large as the mean value itself, so that for a Hubble constant of 50 km s^{-1} Mpc^{-1} the value for the model Galaxy is only one standard deviation from the mean. In the standard model, the disk's M/L value is independent of distance from the galactic center, but increases with distance z from the plane. One finds $M/L = 2.5$ at $z = 0$, 15 at $z = 1$ kpc, and an asymptotic value of 20 for large z. The value of M/L for the spheroid is 1.7, which is comparable to the mean value of 1.6 found for globular clusters (Illingworth 1976) and also the value of 1.8 expected for an elliptical galaxy with an absolute magnitude of -18.4, according to the empirical relation between M/L and luminosity found by Faber and Jackson (1976), assuming a Hubble constant of 100 km s^{-1} Mpc^{-1}. The M/L value for the disk plus spheroid is 4.

In Figure 10, the fraction of the total mass of luminosity contained within a radius r of the galactic center has been plotted for each component separately. The ratio of the spheroid mass contained within r to the disk mass contained within r has been plotted as a solid line in the figure. The corresponding ratio of contained luminosities is a constant factor of 2.5 larger than the ratio of masses. The spheroid contains 6% of the total mass, and 15% of the total luminosity.

c) *The Rotation Curve*

We compute next the rotation curve in the plane of the disk using the conventional two-component mass distribution of the standard Galaxy model (Table 1). We show that dynamical observations require the existence of a third mass component. In § VI, we shall recompute the rotation curve taking account of the additional mass that is expected to exist in the form of a massive halo.

The two-component rotation curve can be calculated by combining the relation found by Freeman (1970) for the rotation of an infinitely thin exponential disk with the Newtonian relation for a spherical mass distribution. One has

$$v_{\rm rot}(r) = \left(\frac{G}{r}\right)^{1/2} \{\mathcal{M}_s(\leq r) + 4\mathcal{M}_d s^3 \times [I_0(s)K_0(s) - I_1(s)K_1(s)]\}^{1/2},$$

$$s = \tfrac{1}{2} r/h, \qquad (20)$$

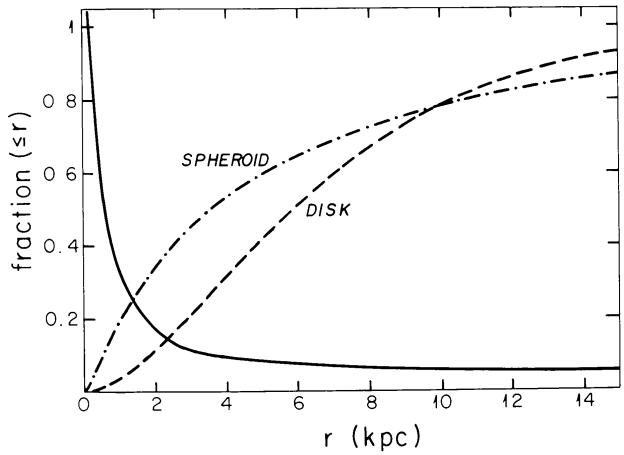

FIG. 10.—The fraction of the total mass or luminosity contained within a radius r of the galactic center for the disk (*dashed line*) and for the spheroid (*mixed dots and dashes*). The ratio of the spheroid mass contained within a radius r to disk mass contained within r has been plotted as a solid line. The corresponding ratio of contained luminosities is a constant factor of 2.5 larger than the ratio of masses.

where $\mathcal{M}_s(\leq r)$ is the enclosed spheroidal mass as a function of radius r, $\mathcal{M}_d$ is the total mass, I and K are modified Bessel functions, and h is the scale length in the plane of the disk. Since the half-thickness of the disk is ~ 300 pc, the thin-disk approximation is very good (relative error $\approx [H/h]\exp[-r/h]$; Newman 1980), except near the galactic center.

The rotation curve is shown in Figure 11. The solar rotation velocity for the two component model is 170 km s^{-1}, significantly lower than the value of ~ 235 km s^{-1} derived from the observed Oort constants. The Oort constants of rotation for the standard model are $A = 11.1$, $B = -9.8$, in disagreement with those found by Oort and Plaut (1975), $A = 16.9 \pm 0.9$ and $B = -9.0 \pm 1.5$, based on a careful weighting of available data.

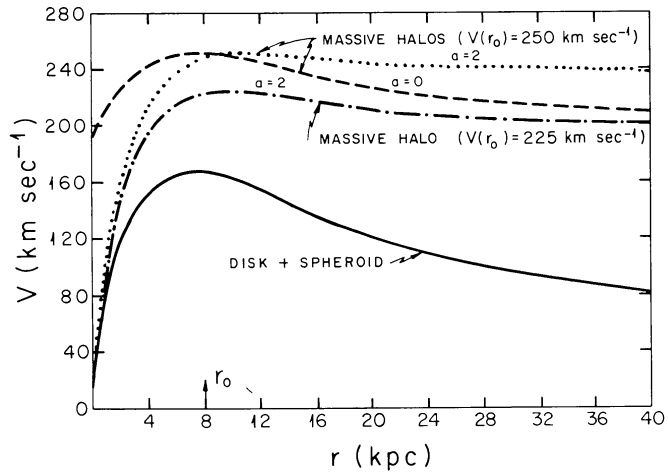

FIG. 11.—The rotation curve in the plane of the disk for the two-component standard Galaxy model (see Table 1) is shown as a solid line. Three illustrative models with massive halos defined by eq. (22) and the parameters indicated in the text are also shown.

(The values adopted by Schmidt [1965] are $A=15\pm1.5$ and $B=-10\pm2$, and those inferred by Gunn, Knapp, and Tremaine (1979) from H I observations are $A=13\pm2$ and $B=-13\pm2$.) The value of Ar_0 for the standard model, 90 km s^{-1}, is to be compared with the range, 120–150 km s^{-1}, found from 21 cm observations (Oort and Plaut 1975). (The values of Ar_0 given by Schmidt [1965] are 135–150 km s^{-1}; those given by Gunn *et al.*, are 105–115 km s^{-1}.)

The rotation constants A, B, and Ar_0 are sensitive to the value of the scale length h assumed for the disk. We find for a two-component model with $h=2.75$ kpc, the rotation constants 16.2, −10.5, and 130, which represent a satisfactory compromise among the above-mentioned three sets of rotation constants at r_0. The solar rotational velocity for this model is 215 km s^{-1}.

The escape velocity in the plane of the disk of the model Galaxy can be calculated by equating at each point the gravitational attraction to the centrifugal force. One has

$$V_{\rm esc}{}^2(r)=2\int_r^\infty \frac{V_{\rm rot}{}^2(R)}{R}\,dR, \qquad (21)$$

where $V_{\rm esc}(r)$ is the escape velocity from a point in the plane of the disk a distance r from the galactic center, and $V_{\rm rot}$ is given by equation (20). The computed values are given in Table 4; they do not include, of course, the effect of a massive halo.

The shape of the rotation curve for the model Galaxy should be compared to that measured for other galaxies of similar morphological type (Rubin, Ford, and Thonnard 1978; Bosma 1978), i.e., a gentle rise to a maximum rotation speed of ~235 km s^{-1}, followed by a dip and then a flat or slightly increasing region out to $\gtrsim$30 kpc. (We are not aware of any published rotation curves that show a monotonically decreasing rotation velocity as expected in the Keplerian limit.) For the Galaxy, Gunn *et al.* find that the rotation curve is flat to at least 25 kpc. The maximum rotation velocity for the standard model is only 170 km s^{-1}. Also the rotation curves of all the two-component models we have constructed based on observed stars fall monotonically beyond 12 kpc, whereas the observations for other galaxies suggest the curve should flatten in this region. These discrepancies suggest the existence of a third mass component of the Galaxy, which we consider next.

VI. THE HALO

Dynamical studies based on virial motions of clustered galaxies (Zwicky 1933) and on galaxy rotation curves (Roberts 1976) have suggested the existence of a third halo component of the galaxy (Oort 1965*a*; Truran and Cameron 1970; Ostriker, Peebles, and Yahil 1974; Einasto, Kaasik, and Saar 1974). This component is often referred to as a massive halo. The results of § V*c* are consistent with this suggestion and are essentially a formal restatement of some of the arguments that led previous authors to propose the existence of a massive halo for the Galaxy.

We construct an illustrative model of a massive halo that is motivated by the observations of the rotation curves of other galaxies. We assume a mass density of the form

$$\rho_{\rm H}(r)=\frac{\rho_{\rm H}(0)}{1+(r/a)^2}, \quad a\neq 0,$$

$$=\frac{\rho_{\rm H}(r_0)}{(r/r_0)^2}, \quad a=0, \qquad (22)$$

where a is the core radius. (The density must eventually fall faster than r^{-2} in order that the total mass be finite. The precise region in which this cutoff occurs is unknown, but does not play a significant role in our discussion.) We will first discuss in § VI*a* the dynamical effects of massive halos of the form given in equation (22) and then outline in § VI*b* the observable implications for the star counts.

a) Dynamical Effects

The rotation velocity that would be observed if only the halo mass were present is

$$V_{\rm H}(r)=V(\infty)\left(r/\sqrt{3}\,a\right), \quad r\ll a,$$

$$=V(\infty), \quad r\gg a, \qquad (23)$$

where $V(\infty)=(4\pi G\rho_{\rm H}(0)a^2)^{1/2}$.

The value of $\rho_{\rm H}(0)a^2$ may be constrained by the requirement that the asymptotic rotation velocity in the halo lie between 175 km s^{-1} and 350 km s^{-1}, as appears to be true in the relevant distance range ($r\lesssim$30 kpc) for nearly all spiral galaxies (Rubin, Ford, and Thonnard 1978; Bosma 1978). This constraint on $V_{\rm H}(\infty)$ corresponds to the following inequality:

$$0.6\leq\left[\left(\frac{\rho_{\rm H}(r_0)}{0.01\mathcal{M}_\odot\ {\rm pc}^{-3}}\right)\left(\frac{r_0{}^2+a^2}{100\ {\rm kpc}^2}\right)\right]\leq 2.3, \qquad (24)$$

where for convenience we have expressed equation (24) in terms of the halo density in the solar neighborhood, $\rho_{\rm H}(r_0)$. It follows from equation (24) that

$$\rho_{\rm H}(r_0)\lesssim 0.035\mathcal{M}_\odot\ {\rm pc}^{-3}, \qquad (25)$$

which is considerably smaller than the total mass density, $0.15\,\mathcal{M}_\odot$ pc^{-3}, in the solar neighborhood. The upper limit of equation (25) is also less than the density of dark matter, $0.06\,\mathcal{M}_\odot$ pc^{-3}, in the solar neighborhood.

The halo parameters, $\rho_{\rm H}$ and a, can be chosen so that the local rotation constants computed from the

three-component model agree with the measured rotation constants, and also so that the calculated rotation curve is approximately flat out to ~40 kpc (§ V). For the standard model disk and spheroid, (see Table 1), these constraints imply $a \lesssim 4$ kpc.

Figure 11 shows three computed rotation curves that include a massive halo. The dashed curve corresponds to a halo with $\rho_H(r_0) = 0.011 \mathcal{M}_\odot$ pc^{-3} and $a = 0$, which we adopt as our standard halo. Also shown in Figure 11 are the rotation curves for a somewhat more massive halo with a larger scale length: $\rho_H(r_0) = 0.017 \mathcal{M}_\odot$ pc^{-3} and $a = 2$ kpc (*dotted line*), and for a halo with $\rho_H(r_0) = 0.010 \mathcal{M}_\odot$ pc^{-3} and $a = 2$ kpc (*mixed dots and dashes*). The amount of dark matter assigned to the disk and spheroid was reduced in the models in order to keep the total local mass density constant at $0.15 \mathcal{M}_\odot$ pc^{-3} (*cf.* § V*b*).

The values for $\rho_H(r_0)$ in the above halo models are smaller than the density of dark (missing) matter of $0.06 \mathcal{M}_\odot$ pc^{-3} in the solar neighborhood. Strongly oblate halos with ellipticity ε of 0.5 (axis ratio of 2:1) could conceivably account for one-third to one-half of the dark matter, but there is no other indication of such highly flattened halos. These considerations also suggest (see § V*b*) that *most of the dark matter in the solar neighborhood is associated with the disk component*.

The rotation constants for the standard halo with $a = 0$ are: $A = 16.1$ km s^{-1} kpc^{-1}, $B = -15.4$ km s^{-1} kpc^{-1}, $Ar_0 = 130$ km s^{-1}, and a solar rotational velocity of 250 km s^{-1}. For the halos with $a = 2$ kpc, the rotation constants are: 13.3, −14.7, 105, and 225 for $\rho_H(r_0) = 0.010$; and 14.4, −17.7, 115, and 250 for $\rho_H(r_0) = 0.017$, respectively. The model values represent a good compromise to the range of observed values of rotation constants reviewed in § V. (The condition $A \approx -B$, implies that the rotation curve is flat near the Sun, as suggested by Gunn *et al.*)

The local halo mass density corresponds to ~10% of the total mass density in the solar neighborhood for each of the halo models discussed above. The total halo mass interior to the Sun's position ($r \leq r_0$) implied by the two model halos with $\rho_H(r_0) > 0.010$ is about two-thirds of the total contained mass within r_0, and about half of the total contained mass for the halo with $\rho_H(r_0) = 0.010$. A halo with this large a mass might stabilize the disk component against barlike modes (Ostriker and Peebles 1973).

The inferred properties of the halo parameters are sensitive to the assumed disk scale length, h. For example, a two-component standard model (cf. Table 1) with a scale length $h = 2.75$ kpc, a halo with $\rho_H(r_0) = 0.0025 \mathcal{M}_\odot$ pc^{-3} and $a = 25$ kpc yields acceptable rotation constants: $A = 15.8$ km s^{-1} kpc^{-1}, $B = -11.7$ km s^{-1} kpc^{-1}, $Ar_0 = 125$ km s^{-1}, and a solar rotational velocity of 220 km s^{-1}, as well as a reasonably flat rotation curve to 40 kpc. The total mass interior to the Sun's position in this halo component is only 10% of the total contained mass within r_0. Halos that do not conflict with available observations can be constructed for essentially all values of a if $h = 2.75$ kpc, which is unlike the situation with $h = 3.5$ kpc (for which $a \lesssim 4$ kpc).

b) *Halo Star Counts*

We consider next how a massive halo may affect the star counts in the direction of the galactic pole. The assumed halo density (eq. [22]) is constant at $b = 90°$ within a factor of order 2 for distances closer than ~10 kpc from the Sun. Therefore, the star densities predicted by the model halos will increase approximately as $10^{0.6m}$ (eq. [26], below) for the apparent magnitude region $m \leq 15 + M_{\text{bright}}$, provided the halo does not contain many stars brighter than M_{bright}. This increase in halo counts with magnitude is much more rapid than for the disk and spheroid. *If at any specified magnitude the halo contributes a sizeable fraction to the counts, then the halo will dominate the counts for all fainter magnitudes*. This rapid increase is not observed in the data for $m_V \lesssim 21$ mag. (A rapid increase is reported by Tyson and Jarvis [1979] for $m_V \gtrsim 21$, but not by Kron [1978] or Peterson *et al.* [1979]. For $m_V \gtrsim 22.5$ mag the Kron data show a rapid increase, but this is caused mainly by contamination by galaxies. See the discussion in § III*c*, and below.) Hence the halo can make only a small contribution to the star counts in the available data region $m_V \lesssim 21$.

The number density, $\mathcal{N}_H(\leq m)$, of halo stars per square degree visible to apparent magnitude m is, for the illustrative case in which all the stars in the halo (with $a = 0$) have the same absolute magnitude, M_0:

$$\mathcal{N}_H(\leq m) = 1.0 \times 10^{-4} (\rho_H(r_0)/\mathcal{M}(M_0)) \times z_{\max}{}^3 \left[3(x_0 - \arctan x_0/x_0{}^3)\right], \quad (26)$$

where $x_0 = (z_{\max}/r_0)$ and $\log(z_{\max}/10 \text{ pc}) = 0.2(m - M_0)$. The quantity in the brackets on the right hand side of equation (26) lies between 0.5 and 1.0 for $z_{\max} \leq 10$ kpc (i.e., $m - M_0 \leq 15$).

The halo star density to $m_V = 21$ mag must be less than or order of one-third the total observed star density since there is no evidence of a rapid increase ($\sim 10^{0.6m}$) in the measured star counts for $m_V \leq 21$ mag (see Fig. 4). This observational constraint implies, for the illustrative case in which the halo stars have a unique luminosity M_V, that

$$M_V{}^{\text{MS}} \gtrsim 12.5 \text{ mag}, \quad (27a)$$

and

$$M_V{}^{\text{WD}} \gtrsim 11.5 \text{ mag}. \quad (27b)$$

In deriving equations (27) we assumed the standard

halo ($\rho_H(r_0)=0.011\mathcal{M}_\odot$ pc^{-3} and $a=0$, (eq. [22]), as well as $\mathcal{M}_{MS}$ ($M_V=12.5$ mag)$=0.2\mathcal{M}_\odot$, as suggested by equation (12), and $\mathcal{M}_{WD}=0.65\mathcal{M}_\odot$. These limiting absolute magnitudes depend upon the logarithm of the assumed stellar mass, $\mathcal{M}$, and halo density, $\rho_H(r_0)$. For a different mass $\mathcal{M}'$ and halo density ρ_H', the limiting absolute magnitude becomes

$$M(\mathcal{M}', \rho_H') = -1.67 \log\left[\frac{\mathcal{M}'\rho_H(r_0)}{\mathcal{M}\rho_H'(r_0)}\right] + M[\mathcal{M}, \rho_H(r_0)]. \quad (28)$$

The maximum luminosity of halo stars can be further constrained by using the $(B-V)$ color distributions in SA 57 and SA 68 (Figs. 8*c* and 8*d*). The previous results show that $B-V$ must be greater than 1.6 if the halo is composed of main-sequence type stars (i.e., they are later than M5). The agreement between the model and the observed star counts, at two latitudes indicate that no more than one-third of the red stars with $19.75 \leq m_V \leq 22.0$ and $(B-V) \geq 1.1$ in SA 57 and SA 68 are halo stars. This implies $M_V{}^{MS} \gtrsim 14.0$ mag and $M_V{}^{WD} \gtrsim 13.0$ mag.

The star counts of Tyson and Jarvis (1979) increase abruptly dimward of $m_V=21$ mag (§ III*c*, and Fig. 4*a*). This behavior might be caused by a just-visible galactic halo, but further observational work is required before one can be sure of the correct interpretation (and establish that it is not due to some unknown systematic error). In order to decide whether a steep rise in the star counts at faint magnitudes is due to a new halo population, to QSOs, or to an increase in the luminosity function of either the disk or spheroid for absolute magnitudes fainter than included in the currently available data (§ III*b*, above), it will be necessary to examine the variation in counts with color and with longitude and latitude. Equation (27a) implies that main-sequence halo stars will have $(B-V)$ colors $\gtrsim +1.6$ (Johnson 1965). If they are much redder than this value they will be redder than the disk stars and should clearly stand out in a $(B-V)$ diagram (Figs. 8*b*, 8*c*, and 8*d*). If the halo stars have $(B-V)$ colors of $\approx +1.6$, comparable to the disk stars, the latitudinal dependence of stars with this color should abruptly change for dim limiting magnitudes as the halo stars begin to contribute significantly to the counts. Single color (two-band) diagrams will be less useful in revealing halo white dwarfs, because white dwarfs have a broad color distribution. Multiple color diagrams (appropriately chosen) should make possible the separation of all the expected components.

The halo star population must be very different from either the disk or spheroidal populations. Main-sequence stars earlier than about M6 cannot be the dominant population of the halo ($M_V{}^{MS} \gtrsim 14.0$ mag, above). The halo could be made up of gray and black dwarfs, but not brighter white dwarfs ($M_V{}^{WD} \gtrsim 13.0$ mag, above). (Dekel and Shaham [1979] suggest that the outer regions of NGC 4565 may consist primarily of nonluminous stars of mass $0.03\mathcal{M}_\odot$.) The cameras on the Space Telescope are expected to be sensitive to magnitudes as faint as $m_V \approx 28$ (Bahcall and O'Dell 1979; Westphal *et al.* 1979; Macchetto and Laurance 1977; Longair 1979). Thus the ST cameras would reveal the stars from a standard massive halo if they are brighter than about

$$M_V(\mathcal{M}) = 19.0 \text{ mag} - 1.67 \log[\mathcal{M}/0.1\mathcal{M}_\odot]. \quad (29)$$

Faint main-sequence type stars could be detected by ST cameras down to limiting absolute magnitudes $M_V{}^{MS} \lesssim 19.0$ mag. Halo white dwarfs would be detectable in the Visible band if $M_V{}^{WD} \lesssim 17.5$ mag. The sensitivity of ST observations to halo stars could be further improved by examining the color distributions of the observed stars.

The brightness limit for both main-sequence ($M_V \gtrsim 14.0$ mag) and white dwarf ($M_V \gtrsim 13.0$ mag) stars implies that the M/L value for the halo must be greater than ~ 650.

The constraints derived above for the brightness of the halo in the Galaxy are comparable to those that have been placed on the halos of other galaxies. For example, in NGC 4565 the halo has a visual surface brightness less than ~ 28 mag arcsec^{-2} (Spinrad *et al.* 1978; Kormendy and Bruzual 1978). For the model halo defined by equation (22), the limits inferred above from star counts for either main-sequence or white dwarf stars ($M_V \gtrsim 12$) correspond to ~ 27 mag arcsec^{-2} for a line of sight that passes 20 kpc from the galactic center. If the standard model halo extends to 50 kpc, the halo could contribute as much as 10% of the total luminosity of the Galaxy for the brightness limits discussed above. The total mass would be $5.0 \times 10^{11}\mathcal{M}_\odot$, 90% from the halo ($\rho_H(r_0)=0.011\mathcal{M}_\odot$ pc^{-3} and $a=0$). The total mass to (disk plus spheroid) luminosity ratio would be 35 (Visual). (For the model with $h=2.75$, the implied values of M_V, surface brightness of the halo, M/L, *etc.*, are about the same as those for the standard, $h=3.5$ kpc, model.)

The illustrative results cited above can be extended easily to the more realistic case of a broad luminosity function for halo stars. In a magnitude-limited survey, there is a most probable absolute luminosity, M_p, for visible stars arising from the combined effects of a maximum brightness for stars, together with the fixed volume of space that is sampled. The results of equations (27) apply for $M_p \approx M_V$. For a typical disk luminosity function with a shape given by equation (1), $M_p \approx M^*$. For a flat luminosity function [$\phi(M)=K$, $M \geq M_0$; $\phi(M)=0$, $M < M_0$], $M_p \approx M_0 - 2$.

VII. DISCUSSION AND APPLICATIONS TO SPACE TELESCOPE OBSERVATIONS

The standard two-component (disk plus spheroid) model of the Galaxy (Table 1) described in this paper is consistent with all of the established data on star densities and $(B-V)$ colors. The assumed global distributions of the stellar disk and spheroid are suggested by observations of other galaxies, while the adopted stellar luminosity functions and scale heights in the disk are determined by measurements in the Galaxy. The known kinematic properties of the Galaxy and a flat rotation curve at large distances can be reproduced if a third component, a massive halo, is added to the standard two-component model. The following remarks review some of our main results for Visual magnitudes (Blue magnitudes are discussed in Appendix A) and indicate some applications to observations with the Space Telescope and ground-based telescopes.

1) The standard model (Table 1) yields characteristic parameters for the disk and spheroid components of the Galaxy (such as the mass and luminosity contained within various radii, the escape velocity, and the total angular momentum in the disk; see Tables 1 and 4). In addition, many detailed properties are specified by the model; e.g., the distributions of visible stars with distance from the Sun (Fig. 7), in absolute magnitude (Fig. 8*a*), and in $(B-V)$ color (Fig. 8*b*). The calculated M/L ratio for the disk and spheroid (5 and 1.7, respectively, in solar units) are in agreement with observations on other Sbc galaxies as are the total luminosity ($M_V=-20.5$, $M_B=-20.1$) and the disk and spheroid scale lengths ($h=3.5$ kpc and $r_e=2.7$ kpc, respectively). If the Hubble constant is 100 km s^{-1} Mpc^{-1} the above-stated values for the Galaxy agree with the mean observed values for other Sbc galaxies. If the Hubble constant is 50 km s^{-1} Mpc^{-1}, these values for the Galaxy are typically one standard deviation from the mean observed values.

2) The calculated star densities due to the conventional disk and spheroidal components agree well with the available data on the latitudinal, longitudinal, and magnitude dependences of the star counts. The total expected number of stars per square degree is about 10^4 deg^{-2} to $m_V=28$ at the galactic pole. This corresponds to only about 25 stars to $m_V=28$ mag in one field at the galactic pole (2.'67 × 2.'67 at $f=12.9$) of the Wide Field Camera of the ST, and only about 0.1 stars on the average per field in the highest resolution mode ($f/96$) of the ST Faint Object Camera. The predictions of the model for the latitudinal and longitudinal dependence of the star counts, as well as their dependence on limiting magnitude, are summarized in Fig. 4–6 and in convenient numerical form in Tables 5 and 6 of Appendix B. Simple formulae that reproduce the predicted model star densities are also provided in Appendix B. When the actual observed numbers of stars at faint magnitudes are available from ST observations, the model results can be used to test, by comparison, whether new stellar populations have been discovered.

3) The available data on star counts and $(B-V)$ color distributions indicate that the spheroid component is approximately spherical, with an ellipticity $\varepsilon \lesssim 0.15$. The data are consistent with a de Vaucouleurs density relation for the spheroid. The Hubble relation is unsatisfactory at approximately the three sigma level of significance. Further data should be obtained with ground-based telescopes (at $m_V \approx 21$ mag) prior to the launching of the ST since the spheroid stars are much more numerous than disk stars at the limiting magnitudes of the ST cameras. Moreover, relatively little observational information is available to date on the spheroid. The appropriate regions for determining spheroid parameters lie in the $l=(0°, 180°)$ and $l=(90°, 270°)$ planes. The best latitudes are $\sim 45°$ and $90°$.

4) The scale length of the disk could be measured also with the aid of ground-based surveys of moderately faint star counts (e.g., $20 \lesssim m_V \lesssim 23$ mag) at relatively large galactic longitudes, $l \gtrsim 120°$, and intermediate galactic latitudes ($b \approx 30°$). The expectations for the latitudinal and longitudinal dependence of the disk counts are summarized in Figure 6*b* and equation (13a).

5) The predicted star counts are insensitive to many of the model parameters (see § IV and Table 3). However, drastic changes in the shape of the luminosity functions of the disk or spheroid outside the magnitude range observed thus far could produce measurable departures from the predicted star counts at faint magnitudes (§ IV*a*). A hole in the stellar distribution in the inner several kiloparsecs of the Galaxy would not be detectable.

6) The distribution of $(B-V)$ colors is double peaked for $18 \lesssim m_V \lesssim 24$ at intermediate to high galactic latitudes. $(B-V)$ colors alone can be used to separate the disk and spheroid stars. In the regime where the distribution is double peaked, most stars with $(B-V) \lesssim 1$ are in the spheroid and most with $(B-V) \gtrsim 1$ are in the disk. The disk stars in a magnitude-limited sample at high galactic latitudes are significantly *redder* than spheroid stars because of the sharp density gradient in the disk.

7) The entire body of astronomical data reviewed here is consistent with, among other things, the following two assumptions: (*a*) there are no populous intermediate scale-height ($\gtrsim 1$ kpc) disk populations; and (*b*) the stellar luminosity functions are independent of position in the Galaxy. The distribution of $B-V$ colors discussed in § III*h* and § IV*d* (see also Fig. 8) is, for example, inconsistent with an intermediate scale-height disk population that contains more than 5% of the local number density of stars in the normal disk component. The constraints on possible variations with position in

the Galaxy of the luminosity functions are less stringent since the star counts are not sensitive to changes in the luminosity function of the disk that occur beyond $\sim$1 kpc or beyond $\sim$10 kpc for the spheroid (see Fig. 7).

8) The $(B-V)$ colors of faint stellar objects ($m_B \approx 23$ mag) indicate that the quasar number density on the sky is much less (by almost two orders of magnitude) than is suggested by an extrapolation of the existing number-magnitude relation for quasars in the range $16 \lesssim m_B \lesssim 20$ mag.

9) The rotation curve computed from the standard two-component Galaxy model is not flat at large distances. A halo with even a relatively small mass density in the solar neighborhood, $\rho_H(r_0) = 0.01 \mathcal{M}_\odot$ pc^{-3}, can give rise to a flat rotation curve (§ VI*a*). The halo parameters necessary to fit the dynamical observations are sensitive to the assumed disk scale length. Most of the dark matter in the solar neighborhood is probably in the disk component.

The stellar content of a massive halo would be revealed by ST observations at $m_V = 28$ if (see eq. [29]) the stars constituting the halo are main-sequence type stars with $M_V \lesssim 19.0$ mag (or faint white dwarfs with $M_V \lesssim 17.5$ mag). The ST sensitivity to halo stars could be further increased by examining the color distributions of the observed stars. Available observations constrain the halo stars to have $M_V \gtrsim 14.0$ mag if they are faint main-sequence stars (and $M_V \gtrsim 13.0$ mag for white dwarfs). Further ground-based observations, especially in the range $21 \lesssim m_V \lesssim 23$ mag, are necessary to determine the significance of the increase in star counts in this magnitude range reported by Tyson and Jarvis (1979). Studies of the dependence of any observed excess number of star counts on magnitude and on latitude and longitude, as well as color, can determine whether the excess is due to; QSOs, a new population of halo stars, a modification of the assumed spheroid density law, or a dramatic increase in the dim end of the disk or spheroid luminosity functions beyond the presently available data.

10) The upward fluctuations of the sky and detector noise will cause a large number of false stars to appear on deep pictures. It is of interest to calculate the magnitude of this effect for the typical conditions that may apply for Space Telescope (and Palomar Sky Survey) observations. Let m be a typical limiting magnitude at which is it specified that a star can be detected at a certain significance level, or S standard deviations above noise. Also let R^2 be the total number of pixels in a field, $N(m)$ the number of real stars that are present on a single picture, and ϵ the required ratio of noise stars to real stars. Finally, let $P(\geq X)$ be the probability (measured in standard deviations) of a noise fluctuation as large as X. Then the loss, Δm, of limiting magnitude below the typical magnitude m can be calculated from the relation

$$P(\geq S \times 10^{0.4\,\Delta\text{mag}}) = \epsilon R^{-2} N(m - \Delta m). \quad (30)$$

For the Wide Field/Planetary Camera it is reasonable to use $m \approx 28$ mag, $N(m) \approx 25$, $S = 3$, and $R = 1600$. If we require that only one in ten apparent stars be a noise fluctuation, then $\epsilon \approx 0.1$. Thus the loss, Δm, of limiting magnitude in the Wide Field/Planetary Camera will be approximately 0.5 mag. The corresponding number for the Faint Object Camera is slightly larger (because of the smaller number of expected stars), i.e., $\Delta m \approx 0.6$ mag. For Palomar Sky Survey plates, the typical loss in limiting magnitude is only of order $\Delta m = 0.3$ mag (for $N(21) \approx 8 \times 10^4$, $R \approx 1 \times 10^4$, and $S = 3$). (The effect calculated here is larger for galaxies, which are spread over many pixels, and will be discussed in more detail in Paper II of this series.)

It is a great pleasure to acknowledge many valuable comments and suggestions by G. de Vaucouleurs, R. G. Kron, J. H. Oort, J. P. Ostriker, M. Schmidt, S. D. Tremaine, and S. van den Bergh. J. H. Oort provided important additional comments in his referee's report. We are grateful to C. R. O'Dell for his encouragement in the undertaking of this series of investigations. This work was supported by NASA contract NAS8-32902.

APPENDIX A

We present in this appendix the calculated star densities in the Blue band obtained with the standard (disk plus spheroid) model Galaxy described in Table 1 (main text). The calculations of § II and § III were repeated with a stellar luminosity function and an obscuration constant that are appropriate to the B band. Since the ideas and methods used are the same as were described in the main text for the V band calculations, we only summarize briefly here the parameters that differ from those used in the Visual band calculation in § II and § III.

Figure 12 is a plot of the B band luminosity functions of McCuskey (1966), Luyten (1968), and van Rhijn (1936). The solid line is the fitted analytic luminosity function in equation (1) with $n_* = 2.55 \times 10^{-3}$, $M^* = +2.20$, $M_b = -6$, $M_d = +19$, $\alpha = 0.60$, $\beta = 0.05$, and $1/\delta = 2.30$.

The scale at the top of Figure 2 (main text) indicates the scale heights of stars in the disk as a function of absolute Blue luminosity M_B. The scale was converted from the Visual band using the data of Keenan (1963), Harris (1963), and Johnson (1965).

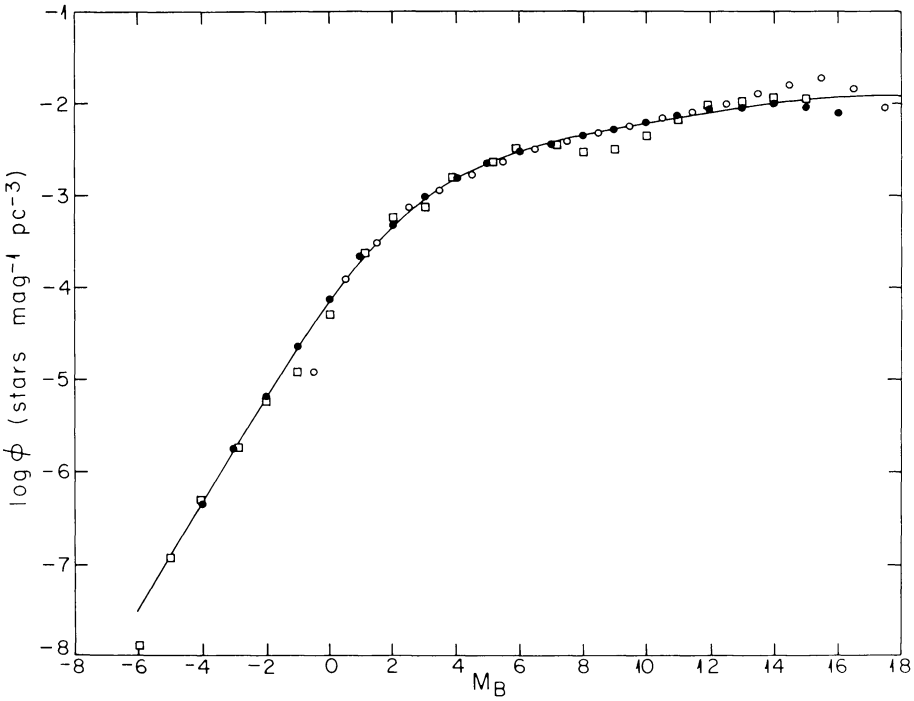

FIG. 12.—Stellar luminosity functions for the disk in the Blue band determined by McCuskey (1966), *filled circles*; Luyten (1968), *open circles*; van Rhijn (1936), *squares*. The solid line is the analytic approximation given in eq. (1) with the parameters listed in Appendix A.

An obscuration constant $A_\infty(90°)=0.20$ (de Vaucouleurs, de Vaucouleurs, and Corwin 1976) was assumed for a cosecant obscuration law (eq. [6]).

Figure 13*a* is a plot of the differential star density, $\mathcal{N}_B$, averaged over longitude for latitudes b of 20°, 30°, 50°, and 90°. We use the relation $m_B=m_{\rm ipg}+0.1$ (de Vaucouleurs, de Vaucouleurs, and Corwin 1976) and equation (10) (to correct the scale error in the Seares *et al.* [1925] data). For the faint counts, we use $m_B=m_J+0.25$ and $m_B=m_{(J+F)/2}+0.80$ (see eq. [12]). The calculated star densities agree well with the observed counts for $m_B\lesssim 22$ mag (cf. the discussion in § III and § VI of the main text).

Figure 13*b* (see also Table 6 of Appendix B) is a plot of the integral star density $\mathcal{N}_B(\leq m)$ averaged over longitude. Figure 14 is a plot of the differential star density $\mathcal{N}_B$ averaged over longitude as a function of latitude. The variation of $\mathcal{N}_B$ with longitude is shown in Figure 15 for latitudes b of 20°, 30°, 50°, and 70°.

The limiting absolute magnitude in B at which halo stars would be revealed can be related to the corresponding limiting V magnitude discussed in § VI by the equation

$$M_B=M_V+(m_B-m_V)+1.67\log\left[\frac{\mathcal{N}(m_V)}{\mathcal{N}(m_B)}\right], \tag{A1}$$

where m_B, m_V are the faintest apparent magnitudes that can be studied and $\mathcal{N}(m_B)$, $\mathcal{N}(m_V)$ are the corresponding integral star densities computed from a standard two-component model. Typical stars at the faintest magnitudes observed so far have $(m_B-m_V)\sim+1$ mag. Since the observed limiting star densities are about the same for the data shown in Figures 4*c* and 13*b*, the limiting absolute magnitudes are related by $M_B\approx M_V+1$. This relation applies to the constraints on halo stars expressed by equation (27). The difference in limiting absolute magnitudes, M_B-M_V that will be achieved with ST cameras will depend primarily on the difference in faintest apparent magnitudes (m_B-m_V) that can be studied, since the integral star counts, predicted with the aid of a standard Galaxy model, are approximately equal at the faintest magnitudes in B and V.

The total Blue luminosities of the disk, spheroid, and disk plus spheroid are $1.4(+10)$, $2.5(+9)$, and $1.7(+10)L_\odot$, respectively. The total absolute Blue magnitude of the Galaxy without obscuration is -20.1 mag (with ${M_\odot}^B=+5.48$). The color index $(B-V)$ for the model Galaxy is $+0.50$ (including a $+0.05$ mag correction for reddening due to obscuration), about what is measured for Sbc galaxies (de Vaucouleurs 1977*b*). The color index $(B-V)$ for the spheroid is $+0.45$, about 0.1 magnitude bluer than is measured for metal poor "halo" globular clusters (van den Bergh 1967; Burstein and McDonald 1975). This may be an indication that the bright end ($M\lesssim 0$) of the luminosity function for the spheroid component has been overestimated somewhat. The model star counts are not affected because stars in this absolute magnitude range contribute negligibly to the counts (Fig. 8*a*).

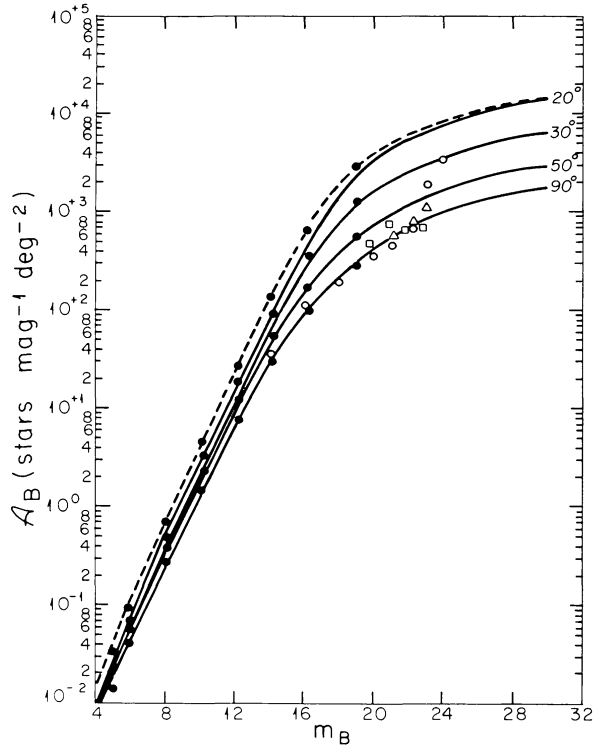

FIG. 13*a*

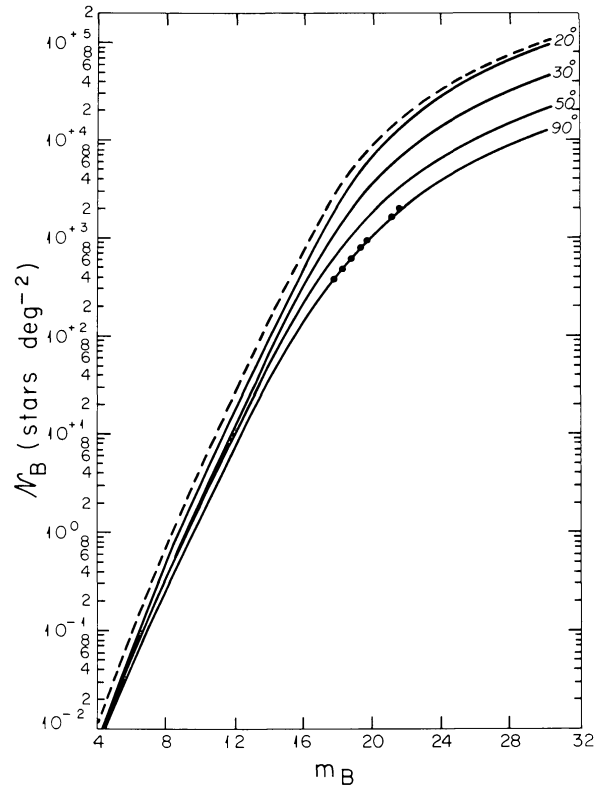

FIG. 13*b*

FIG. 13.—(*a*) The differential star density A_B averaged over longitude (as in Fig. 4*a*) with $A_\infty(90°)=0.20$. (*b*) The integral star density N_B averaged over longitude (as in Fig. 4*c*) with $A_\infty(90°)=0.20$. Data from Brown (1979) are plotted as filled circles.

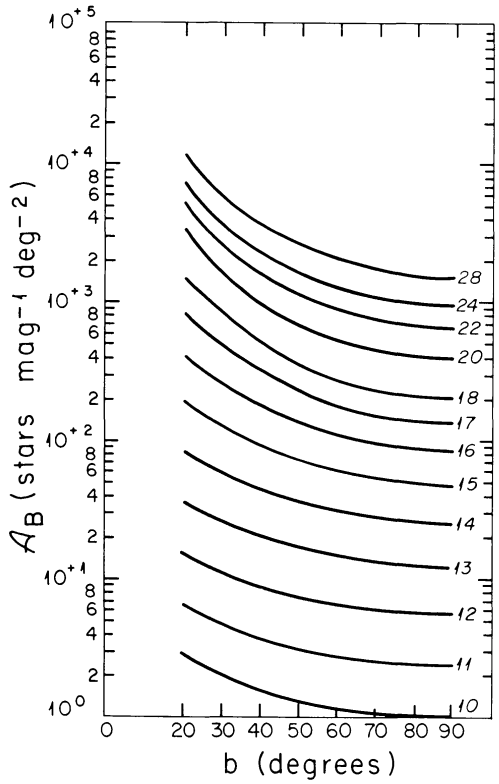

FIG. 14.—The variation of differential star density A_B with latitude b (as in Fig. 5) with $A_\infty(90°)=0.20$

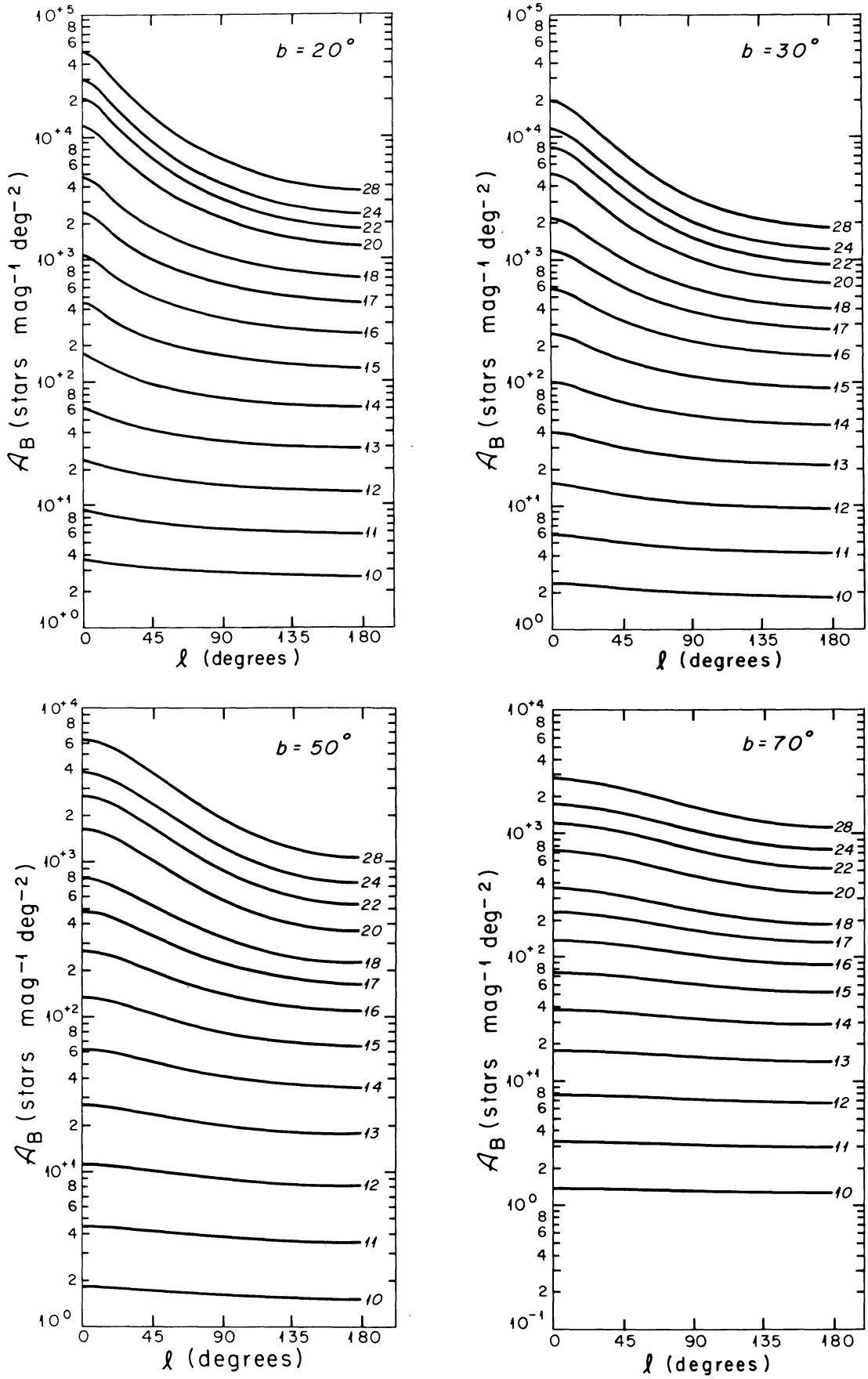

FIG. 15.—The variation of differential star density A_B with longitude (as in Fig. 6*a*) with $A_\infty(90°)=0.20$

APPENDIX B

We present compact formulae that allow one to estimate quickly (using a hand calculator) both the differential and integral star counts for a given galactic longitude, latitude, and apparent magnitude in both V and B over the ranges considered in this paper ($b \geq 20°$, $4 \leq m \leq 30$). We use semiempirical generalizations of equations (13a) and (13b) for the star counts of the disk and spheroid components to estimate the total star counts with zero obscuration, $A=0$. For nonzero obscuration (eqs. [6], [7]), replace m by $(m-A)$ in the formulae below.

The accuracy for the total counts is typically 15% (average absolute error) for the differential counts and integral counts over the 7 orders of magnitude variation in the star densities for the ranges of l, b, and m considered. The units of the differential counts $\mathscr{A}$ are stars per magnitude per square degree, and the units of the integral counts $\mathscr{N}$ are stars per square degree.

$$\mathscr{A}(l,b,m)=\frac{C_1 10^{\beta(m-m^*)}}{[1+10^{\alpha(m-m^*)}]^{\delta}}\,\frac{1}{[\sin b(1-\mu\cot b\cos l)]^{3-5\gamma}}$$

$$+\frac{C_2 10^{\eta(m-m^\dagger)}}{\left[1+10^{\kappa(m-m^\dagger)}\right]^{\lambda}}\,\frac{1}{(1-\cos b\cos l)^{\sigma}}, \tag{B1}$$

where $\mu=0.03$, $(m \leq 12)$, $0.0075(m-12)+0.03$, $(12<m<20)$, $0.09(m \geq 20)$; $\gamma=0.36(m \leq 12)$, $0.04(12-m)+0.36(12<m<20)$; 0.04 $(m \geq 20)$; and $\sigma=1.45-0.20\cos b\cos l$. For $\mathscr{A}_V=\mathscr{A}$,

$$C_1=200, \quad \alpha=-0.2, \quad \beta=0.01, \quad \delta=2, \quad m^*=15;$$

$$C_2=400, \quad \kappa=-0.26, \quad \eta=0.065, \quad \lambda=1.5, \quad m^\dagger=17.5.$$

For $\mathscr{N}_V=\mathscr{A}$,

$$C_1=925, \quad \alpha=-0.132, \quad \beta=0.035, \quad \delta=3.0, \quad m^*=15.75;$$

$$C_2=1050, \quad \kappa=-0.180, \quad \eta=0.087, \quad \lambda=2.50, \quad m^\dagger=17.5.$$

For $\mathscr{A}_B=\mathscr{A}$,

$$C_1=235, \quad \alpha=-0.227, \quad \beta=0.0, \quad \delta=1.50, \quad m^*=17;$$

$$C_2=370, \quad \kappa=-0.175, \quad \eta=0.06, \quad \lambda=2.0, \quad m^\dagger=18.$$

For $\mathscr{N}_B=\mathscr{A}$,

$$C_1=950, \quad \alpha=-0.124, \quad \beta=0.027, \quad \delta=3.1, \quad m^*=16.60;$$

$$C_2=910, \quad \kappa=-0.167, \quad \eta=0.083, \quad \lambda=2.50, \quad m^\dagger=18. \tag{B2}$$

Tables 5 and 6 list the differential and integral star counts at selected longitudes, latitudes, and magnitudes (both V and B) for the standard model that were obtained by direct integration of equation (5). Equation (B1) can be used to accurately interpolate between tabulated values.

APPENDIX C

In this appendix we describe the transformation from absolute magnitude to $(B-V)$ color used in § III*h*.

For the disk population we use the data of Keenan (1963), Harris (1963), and Johnson (1965) for main-sequence stars. We ignore giant-branch stars ($M_V \lesssim +4$) since they make only a negligible contribution for the apparent magnitude intervals considered here (Fig. 8*a* and § II*a*).

For the spheroid stars, the main-sequence is shifted blueward slightly (Roman 1954) due to metal deficiencies that are observed for high velocity stars (Chamberlain and Aller 1951). To calculate the color offset we apply the mean ultraviolet excess, $\langle \delta(U-B) \rangle = 0.20$ mag, for the sample of high velocity stars in Eggen, Lynden-Bell, and Sandage

TABLE 5

DIFFERENTIAL STAR DENSITIES $\mathcal{N}(m)$ PER MAGNITUDE PER SQUARE DEGREE IN THE V AND B BANDS[†#]

	m	b=90°	b=50°			b=30°			b=20°		
			ℓ=0°	90°	180°	ℓ=0°	90°	180°	ℓ=0°	90°	180°
V	10	2.04(0)	2.90(0)	2.66(0)	2.52(0)	3.94(0)	3.43(0)	3.20(0)	5.94(0)	5.00(0)	4.57(0)
B		1.22(0)	1.81(0)	1.61(0)	1.52(0)	2.39(0)	1.99(0)	1.85(0)	3.61(0)	2.86(0)	2.62(0)
V	11	4.91(0)	7.34(0)	6.45(0)	6.02(0)	9.93(0)	8.07(0)	7.40(3)	1.48(1)	1.41(1)	1.03(1)
B		2.88(0)	4.46(0)	3.80(0)	3.53(0)	5.91(0)	4.56(0)	4.18(0)	8.96(0)	6.43(0)	5.79(0)
V	12	1.15(1)	1.88(1)	1.56(1)	1.42(1)	2.63(1)	1.93(1)	1.73(1)	3.93(1)	2.65(1)	2.33(1)
B		6.63(0)	1.12(1)	8.96(1)	8.14(1)	1.52(1)	1.06(1)	9.55(0)	2.31(1)	1.45(1)	1.29(1)
V	13	2.52(1)	4.59(1)	3.51(1)	3.11(1)	7.09(1)	4.54(1)	3.93(1)	1.11(2)	6.27(1)	5.35(1)
B		1.45(1)	2.70(1)	2.00(1)	1.76(1)	3.98(1)	2.46(1)	2.14(1)	6.19(1)	3.32(1)	2.86(1)
V	14	5.03(1)	1.05(2)	7.27(1)	6.18(1)	1.87(2)	1.02(2)	8.46(1)	3.14(2)	1.46(2)	1.19(2)
B		2.95(1)	6.18(1)	4.17(1)	3.54(1)	1.02(2)	5.43(1)	4.55(1)	1.68(2)	7.53(1)	6.23(1)
V	15	9.10(1)	2.22(2)	1.37(2)	1.11(2)	4.63(2)	2.12(2)	1.67(2)	8.46(2)	3.21(2)	2.48(2)
B		5.53(1)	1.33(2)	8.03(1)	6.54(1)	2.51(2)	1.13(2)	9.02(1)	4.44(2)	1.64(2)	1.29(2)
V	16	1.49(2)	4.26(2)	2.28(2)	1.75(2)	1.04(3)	3.98(2)	2.96(2)	2.07(3)	6.52(2)	4.72(2)
B		9.53(1)	2.65(2)	1.41(2)	1.09(2)	5.74(2)	2.17(2)	1.65(2)	1.09(3)	3.35(2)	2.50(2)
V	17	2.25(2)	7.37(2)	3.41(2)	2.47(2)	2.06(3)	6.54(2)	4.59(2)	4.48(3)	1.19(3)	8.00(2)
B		1.50(2)	4.79(2)	2.24(2)	1.64(2)	1.19(3)	3.80(2)	2.73(2)	2.43(3)	6.32(2)	4.43(2)
V	18	3.27(2)	1.17(3)	4.73(2)	3.24(2)	3.56(3)	9.42(2)	6.25(2)	8.40(3)	1.88(3)	1.19(3)
B		2.22(2)	7.81(2)	3.22(2)	2.22(2)	2.17(3)	5.91(2)	4.02(2)	4.77(3)	1.08(3)	7.07(2)
V	19	4.61(2)	1.72(3)	6.33(2)	4.12(2)	5.45(3)	1.23(3)	7.82(2)	1.36(4)	2.59(3)	1.56(3)
B		3.16(2)	1.17(3)	4.36(2)	2.86(2)	3.49(3)	8.18(2)	5.28(2)	8.22(3)	1.62(3)	1.00(3)
V	20	6.23(2)	2.38(3)	8.21(2)	5.13(2)	7.60(3)	1.53(3)	9.41(2)	1.95(4)	3.23(3)	1.89(3)
B		4.30(2)	1.63(3)	5.70(2)	3.59(2)	5.01(3)	1.04(3)	6.48(2)	1.24(4)	2.16(3)	1.28(3)
V	22	1.00(3)	3.85(3)	1.25(3)	7.46(2)	1.22(4)	2.18(3)	1.28(3)	3.12(4)	4.48(3)	2.54(3)
B		7.06(2)	2.69(3)	8.88(2)	5.35(2)	8.33(3)	1.52(3)	9.09(2)	2.10(4)	3.11(3)	1.78(3)
V	24	1.40(3)	5.33(3)	1.70(3)	9.92(2)	1.69(4)	2.86(3)	1.64(3)	4.26(4)	5.78(3)	3.22(3)
B		1.01(3)	3.80(3)	1.24(3)	7.36(2)	1.18(4)	2.07(3)	1.21(3)	2.95(4)	4.15(3)	2.34(3)
V	26	1.77(3)	6.75(3)	2.11(3)	1.20(3)	2.14(4)	3.51(3)	1.97(3)	5.38(4)	7.06(3)	3.87(3)
B		1.32(3)	4.98(3)	1.61(3)	9.42(2)	1.55(4)	2.68(3)	1.55(3)	3.87(4)	5.33(3)	2.98(3)
V	28	2.07(3)	8.07(3)	2.39(3)	1.29(3)	2.58(4)	3.90(3)	2.10(3)	6.51(4)	7.93(3)	4.22(3)
B		1.59(3)	6.20(3)	1.91(3)	1.06(3)	1.96(4)	3.24(3)	1.81(3)	4.91(4)	6.57(3)	3.61(3)
V	30	2.24(3)	8.97(3)	2.40(3)	1.18(3)	2.91(4)	3.66(3)	1.75(3)	7.40(4)	7.57(3)	3.74(3)
B		1.79(3)	7.28(3)	1.96(3)	9.69(2)	2.36(4)	3.23(3)	1.61(3)	6.04(4)	7.02(3)	3.58(3)

[†]These numbers were computed using the standard model of Table 1 (main text) with $A_V = 0.15$ and $A_B = 0.20$ (equation 6) for latitudes b of 20° and 30°, and $A_V = A_B = 0$ for latitudes b of 50° and 90°.

#For each apparent magnitude, the numbers on the first line are the star densities in the V-band; the numbers on the second line are the B-band star densities.

(1962) to the relation between color offset $\Delta(B-V)$ and $\delta(U-B)$ determined by Wildey *et al.* (1962). The color offset $\Delta(B-V)\approx-0.15$ for $(B-V)=0.5$. A comparable offset exists for M dwarfs with $(B-V)\gtrsim1.5$ (Greenstein 1965). Hence we set $\Delta(B-V)=-0.15$ for all spheroid stars. Spheroid giant-branch stars make a significant contribution to the star counts for $m_V\lesssim19$. For the giant branch we use the color magnitude relation for M67 (Johnson and Sandage 1955) which resembles that for high velocity stars (Roman 1965).

REFERENCES

Abell, G. O., and Mihalas, D. M. 1966, *A. J.*, **71**, 635.
Arp, H. 1965, *Ap. J.* **141**, 43.
Baade, W. 1944, *Ap. J.*, **100**, 137.
_____. 1951, *Pub. Univ. Michigan Obs.*, **10**, 7.
Bahcall, J. N., and O'Dell, C. R. 1979, in *IAU Colloquium No. 54, Scientific Research With The Space Telescope*, ed. M. S. Longair and J. W. Warner (Washington, D.C.: US Gov. Printing Office), p. 5.

TABLE 6

INTEGRATED STAR DENSITIES $\mathcal{N}(\leq m)$ PER SQUARE DEGREE IN THE V AND B BANDS[†#]

	m	b=90°	b=50°			b=30°			b=20°		
			ℓ=0°	90°	180°	ℓ=0°	90°	180°	ℓ=0°	90°	180°
V	10	2.30(0)	3.19(0)	3.01(0)	2.90(0)	4.21(0)	3.84(0)	3.62(0)	6.23(0)	5.54(0)	5.13(0)
B		1.42(0)	2.03(0)	1.88(0)	1.80(0)	2.56(0)	2.26(0)	2.13(0)	3.76(0)	3.23(0)	2.99(0)
V	11	5.46(0)	7.77(0)	7.13(0)	6.78(0)	1.04(1)	9.09(0)	8.48(0)	1.55(1)	1.31(1)	1.20(1)
B		3.29(0)	4.85(0)	4.34(0)	4.11(0)	6.29(0)	5.27(0)	4.90(0)	9.43(0)	7.53(0)	6.89(0)
V	12	1.31(1)	1.96(1)	1.72(1)	1.16(1)	2.65(1)	2.16(1)	1.98(1)	3.94(1)	3.04(1)	2.74(1)
B		7.68(0)	1.19(1)	1.02(1)	9.50(0)	1.58(1)	1.22(1)	1.12(1)	2.37(1)	1.72(1)	1.55(1)
V	13	3.03(1)	4.91(1)	4.08(1)	3.73(1)	6.97(1)	5.13(1)	4.60(1)	1.05(2)	7.11(1)	6.27(1)
B		1.76(1)	2.94(1)	2.37(1)	2.16(1)	4.04(1)	2.85(1)	2.56(1)	6.14(1)	3.92(1)	3.47(1)
V	14	6.64(1)	1.19(2)	9.20(1)	8.17(1)	1.85(2)	1.20(2)	1.04(2)	2.92(2)	1.67(2)	1.43(2)
B		3.84(1)	7.05(1)	5.29(1)	4.69(1)	1.04(2)	6.52(1)	5.69(1)	1.64(2)	8.93(1)	7.71(1)
V	15	1.35(2)	2.74(2)	1.93(2)	1.65(2)	4.83(2)	2.69(2)	2.25(2)	8.12(2)	3.85(2)	3.16(2)
B		7.92(1)	1.62(2)	1.11(2)	9.56(1)	2.66(2)	1.44(2)	1.22(2)	4.39(2)	2.01(2)	1.67(2)
V	16	2.53(2)	5.86(2)	3.72(2)	3.07(2)	1.19(3)	5.64(2)	4.51(2)	2.15(3)	8.48(2)	6.62(2)
B		1.53(2)	3.52(2)	2.19(2)	1.81(2)	6.49(2)	3.02(2)	2.45(2)	1.14(3)	4.38(2)	3.49(2)
V	17	4.37(2)	1.15(3)	6.54(2)	5.18(2)	2.68(3)	1.08(3)	8.26(2)	5.25(3)	1.74(3)	1.29(3)
B		2.74(2)	7.13(2)	4.00(2)	3.17(2)	1.49(3)	5.93(2)	4.60(2)	2.79(3)	9.06(2)	6.86(2)
V	18	7.09(2)	2.09(3)	1.06(3)	8.02(2)	5.43(3)	1.88(3)	1.37(3)	1.15(4)	3.26(3)	2.28(3)
B		4.58(2)	1.33(3)	6.71(2)	5.09(2)	3.17(3)	1.07(3)	7.97(2)	6.25(3)	1.74(3)	1.25(3)
V	19	1.10(3)	3.52(3)	1.61(3)	1.17(3)	9.89(3)	2.97(3)	2.07(3)	2.24(4)	5.50(3)	3.65(3)
B		7.24(2)	2.30(3)	1.05(3)	7.62(2)	5.91(3)	1.78(3)	1.26(3)	1.26(4)	3.08(3)	2.11(3)
V	20	1.64(3)	5.56(3)	2.33(3)	1.63(3)	1.64(4)	4.34(3)	2.93(3)	3.89(4)	8.42(3)	5.38(3)
B		1.09(3)	3.69(3)	1.55(3)	1.08(3)	1.01(4)	2.71(3)	1.85(3)	2.29(4)	4.98(3)	3.25(3)
V	22	3.26(3)	1.18(4)	4.39(3)	2.88(3)	3.62(4)	8.03(3)	5.15(3)	8.97(4)	1.61(4)	9.81(3)
B		2.22(3)	7.99(3)	3.00(3)	1.97(3)	2.35(4)	5.26(3)	3.40(3)	5.65(4)	1.03(4)	6.31(3)
V	24	5.66(3)	2.10(4)	7.35(3)	4.62(3)	6.53(4)	1.31(4)	8.08(3)	1.64(5)	2.64(4)	1.56(4)
B		3.94(3)	1.45(4)	5.12(3)	3.24(3)	4.35(4)	8.84(3)	5.51(3)	1.07(5)	1.75(4)	1.04(4)
V	26	8.85(3)	3.31(4)	1.12(4)	6.83(3)	1.04(5)	1.95(4)	1.17(4)	2.60(5)	3.92(4)	2.27(4)
B		6.27(3)	2.32(4)	7.98(3)	4.92(3)	7.07(4)	1.36(4)	8.26(3)	1.75(5)	2.69(4)	1.57(4)
V	28	1.27(4)	4.79(4)	1.57(4)	9.35(3)	1.51(5)	2.70(4)	1.58(4)	3.79(5)	5.44(4)	3.09(4)
B		9.21(3)	3.44(4)	1.15(4)	6.96(3)	1.06(5)	1.95(4)	1.17(4)	2.62(5)	3.89(4)	2.23(4)
V	30	1.70(4)	6.51(4)	2.06(4)	1.19(4)	2.06(5)	3.47(4)	1.98(4)	5.19(5)	7.02(4)	3.91(4)
B		1.26(4)	4.80(4)	1.55(4)	9.03(3)	1.49(5)	2.62(4)	1.52(4)	3.72(5)	5.28(4)	2.98(4)

[†]These numbers were computed using the standard model of Table 1 (main text) with $A_V = 0.15$ and $A_B = 0.20$ (equation 6) for latitudes b of 20° and 30°, and $A_V = A_B = 0$ for latitudes b of 50° and 90°.

#For each apparent magnitude, the numbers on the first line are the star densities in the V-band; the numbers on the second line are the B-band star densities.

Bahcall, J. N., and Sargent, W. L. W. 1967, *Ap. J. (Letters)*, **148**, L65.
Balona, L. A., and Feast, M. W. 1974, *M.N.R.A.S.*, **167**, 621.
Becker, F. 1939, *Zs. f. Ap.*, **19**, 50.
Blaauw, A. 1965, in *Galactic Structure*, ed. A. Blaauw and M. Schmidt (Chicago: University of Chicago Press), p. 435.
Bohuski, T. J., and Weedman, D. W. 1979, *Ap. J.*, **231**, 653.
Bok, B. J. 1937, *The Distribution of Stars in Space* (Chicago: University of Chicago Press).
Bok, B. J., and MacRae, D. A. 1941, *Ann. NY Acad. Sci.*, **42**, 219.
Bosma, A. 1978, Ph.D. thesis, University of Groningen.
Braccesi, A., Zitelli, F., and Formiggini, L. 1980, *Astr. Ap.*, in press.
Brown, G. S. 1979, *A. J.*, **84**, 1647.
Burbidge, G. R., Crowne, A. H., and Smith, H. E. 1977, *Ap. J. Suppl.*, **33**, 113.
Burstein, D., and Heiles, C. 1978, *Ap. J.*, **225**, 40.
Burstein, D., and McDonald, L. H. 1975, *A. J.*, **80**, 17.
Chamberlain, J. W., and Aller, L. H. 1951, *Ap. J.*, **114**, 52.
Chiu, L.-T. G. 1980, preprint.
Dekel, A., and Shaham, J. 1979, *Astr. Ap.*, **74** 186.
de Vaucouleurs, G. 1959, in *Handbuch der Physik*, **Vol. 53**, ed. S. Flügge (Berlin: Springer-Verlag), p. 311.
———. 1977*a*, *A. J.*, **82**, 456.
———. 1977*b*, in *The Evolution of Galaxies and Stellar Populations*, ed. B. Tinsley and R. Larson (New Haven: Yale Univ. Obs.), p. 43.
de Vaucouleurs, G., and Buta, R. 1978, *A. J.*, **83**, 1383.
de Vaucouleurs, G., de Vaucouleurs, A., and Corwin, H. G. 1976, *Second Reference Catalogue of Bright Galaxies* (Austin: University of Texas Press).
de Vaucouleurs, G., and Pence, W. D. 1978, *A. J.*, **83**, 1163.
Eggen, O. J., Lynden-Bell, D., and Sandage, A. R. 1962, *Ap. J.*, **136**, 748.
Einasto, J., Kaasik, A., and Saar, E. 1974, *Nature*, **250**, 309.
Elvius, T. 1951, *Stockholm Obs. Ann.*, **16**, Nos. 4 and 5.
———. 1965, in *Galactic Structure*, ed. A. Blaauw and M. Schmidt (Chicago: University of Chicago Press), p. 41.
Faber, S. M., Burstein, D., Tinsley, B. M., and King, I. R. 1976, *A. J.*, **81**, 45.
Faber, S. M., and Jackson, R. E. 1976, *Ap. J.*, **204**, 668.
Freeman, K. C. 1970, *Ap. J.*, **160**, 811.

Gordon, M. A., and Burton, W. B. 1976, *Ap. J.*, **208**, 346.
Greenstein, J. L. 1965, in *Galactic Structure*, ed. A. Blaauw and M. Schmidt (Chicago: University of Chicago Press), p. 361.
Gunn, J. E., Knapp, G. R., and Tremaine, S. D. 1979, *A. J.*, **84**, 1181.
Harris, D. L., 1963, in *Basic Astronomical Data*, ed. K. Aa. Strand (Chicago: University of Chicago Press), p. 263.
Harris, D. L., Strand, K. Aa, and Worley, C. E. 1963, in *Basic Astronomical Data*, ed. K. Aa. Strand (Chicago: University of Chicago Press), p. 273.
Harris, W. E. 1976, *A. J.*, **81**, 1095.
Heiles, C. 1976, *Ap. J.*, **204**, 379.
Hill, E. R. 1960, *Bull. Astr. Inst. Netherlands*, **15**, 1.
Hoag, A. A., and Smith, M. G. 1977, *Ap. J.* **217**, 362.
Hubble, E. 1930, *Ap. J.*, **71**, 231.
Illingworth, G. 1976, *Ap. J.*, **204**, 73.
Innanen, K. A. 1973, *Ap. Space Sci.*, **22**, 393.
Johnson, H. L. 1965, *Ap. J.*, **141**, 170.
Johnson, H. L., and Sandage, A. R. 1955, *Ap. J.*, **121**, 616.
Keenan, P. C. 1963, in *Basic Astronomical Data*, ed. K. Aa. Strand (Chicago: University of Chicago Press), p. 78.
King, I. R. 1966, *A. J.*, **71**, 131.
Knapp, G. R., Tremaine, S. D., and Gunn, J. E. 1978, *A. J.*, **83**, 1585.
Kormendy, J. 1977*a*, *Ap. J.*, **217**, 406.
_____. 1977*b*, *Ap. J.*, **218**, 333.
Kormendy, J., and Bruzual, A. G. 1978, *Ap. J.* (*Letters*), **223**, L63.
Kron, R. G. 1978, Ph.D. thesis, University of California, Berkeley.
Liebert, J., Dahn, C. C., Gresham, M., and Strittmatter, P. A. 1979, *Ap. J.*, **233**, 226.
Longair, M. S. 1979, *Quart. J. R. A. S.*, **20**, 5.
Luyten, W. J. 1938, *M. N. R. A. S.*, **98**, 677.
_____. 1968, *M. N. R. A. S.*, **139**, 221.
Macchetto, F. and Laurance, R. J. 1977, *The Faint Object Camera*, European Space Agency report SN-126.
Maihara, T., Oda, N., Sugiyama, T., and Okuda, H. 1978, *Pub. Astr. Soc. Japan*, **30**, 1.
McCuskey, S. W. 1966, *Vistas Astr.*, **7**, 141.
Miller, G. E., and Scalo, J. M. 1979, *Ap. J. Suppl.*, **41**, 513.
Morgan, W. W., Harris, D. L., and Johnson, H. L. 1953, *Ap. J.*, **118**, 92.
Newman, W. I. 1980, in preparation.
Oemler, A. 1976, *Ap. J.*, **209**, 693.
Oort, J. H. 1926, *Pub. Kapteyn Astr. Lab. Groningen*, No. 40.
_____. 1932, *Bull, Astr. Inst. Netherlands*, **6**, 249.
_____. 1936, *Bull. Astr. Inst. Netherlands*, **8**, 75.
_____. 1938, *Bull. Astr. Inst. Netherlands*, **8**, 233.
_____. 1960, *Bull. Astr. Inst. Netherlands*, **15**, 45.
_____. 1965*a*, *I. A. U. Trans.*, **12A**, 789.
_____. 1965*b*, in *Galactic Structure*, ed., A. Blaauw and M. Schmidt (Chicago: University of Chicago Press), p. 455.
Oort, J. H., and van Herk, G. 1959, *Bull. Astr. Inst. Netherlands*, **14**, 299.
Oort, J. H., and Plaut, L. 1975, *Astr. Ap.*, **41**, 71.
Osmer, P. A. 1978, *Phys. Scripta*, **17**, 357.
Ostriker, J. P., and Caldwell, J. A. R. 1978, *IAU Symposium No. 84, The Large Scale Characteristics of the Galaxy*, ed. W. B. Burton (Dordrecht: Reidel), p. 441.
Ostriker, J. P., and Peebles, P. J. E. 1973, *Ap. J.*, **186**, 467.
Ostriker, J. P., Peebles, P. J. E., and Yahil, A. 1974, *Ap. J.* (*Letters*), **193**, L1.
Peterson, B. A., Ellis, R. S., Kibblewhite, E. J., Bridgeland, M. T., Hooley, T., and Horne, D. 1979, *Ap. J.* (*Letters*), **233**, L109.
Poveda, A. 1960, *Bol. Inst. Tonantzintla*, No. 17.
Roberts, M. S. 1975, in *Galaxies and the Universe*, ed. A. Sandage, M. Sandage, and J. Kristian (Chicago: University of Chicago Press), p. 309.
_____. 1976, *Comments Ap. Space Phys.*, **6**, 105.
Roberts, M. S., and Whitehurst, R. N. 1975, *Ap. J.*, **201**, 327.
Roman, N. G. 1954, *A. J.*, **59**, 307.
_____. 1965, in *Galactic Structure*, ed. A. Blaauw and M. Schmidt (Chicago: University of Chicago Press), p. 345.
Rubin, V. C., Ford, W. K., Jr., Thonnard, N. 1978, *Ap. J.* (*Letters*), **225**, L107.
Sandage, A. 1954, *A. J.*, **59**, 162.
_____. 1957, *Ap. J.*, **125**, 422.
_____. 1972, *Ap. J.*, **178**, 1.
_____. 1973, *Ap. J.*, **183**, 711.
Sandage, A., and Visvanathan, N. 1978, *Ap. J.*, **223**, 707.
Schmidt, M. 1959, *Ap. J.*, **129**, 243.
_____. 1963, *Ap. J.*, **137**, 758.
_____. 1965, in *Galactic Structure*, ed. A. Blaauw and M. Schmidt (Chicago: University of Chicago Press), p. 513.
_____. 1975, *Ap. J.*, **202**, 22.
_____. 1978, *Phys. Scripta* **17**, 329.
Seares, F. H. 1925, *Ap. J.*, **61**, 114.
Seares, F. H., and Joyner, M. C., 1928, *Ap. J.*, **67**, 24.
Seares, F. H., van Rhijn, P. J., Joyner, M. C., and Richmond, M. L. 1925, *Ap. J.*, **62**, 320.
Simoda, M., and Hiroshi, K. 1968, *Ap. J.*, **151**, 133.
Sion, E. M., and Liebert, J. 1977, *Ap. J.*, **213**, 468.
Solomon, P. M., and Sanders, D. B. 1979, in *Giant Molecular Clouds in the Galaxy*, ed. P. Solomon and M. Edmunds (London: Pergamon Press).
Soneira, R. M. 1980, in prepration.
Spinrad, H., Ostriker, J. P., Stone, R. P. S., Chiu, L. T. G., and Bruzual, A. G. 1978, *Ap. J.*, **225**, 56.
Spitzer, L. 1978, *Physical Processes in the Interstellar Medium* (New York: Wiley).
Spitzer, L., and Schwarzschild, M., 1951, *Ap. J.*, **114**, 385.
Stebbins, J., Whitford, A. E., and Johnson, H. L. 1950, *Ap. J.*, **112**, 469.
Steppe, H., Veron, P., and Veron, M. P. 1979, *Astr. Ap.*, **78**, 125.
Tremaine, S. D., Ostriker, J. P., and Spitzer, L. 1975, *Ap. J.*, **407**, 19.
Truran, J. W., and Cameron, A. G. W. 1970, *Nature*, **225**, 710.
Tyson, J. A., and Jarvis, J. F. 1979, *Ap. J.* (*Letters*), **230**, L153.
Upgren, A. R. 1963, *A. J.*, **68**, 475.
van den Bergh, S. 1967, *A. J.*, **72**, 70.
_____. 1968, *Comm. D. Dunlap Obs.*, No. 195.
_____. 1971, *A. J.*, **76**, 1082.
_____. 1976, *Ap. J.*, **206**, 883.
van Rhijn, P. J. 1936, *Pub. Kapteyn Astr. Lab. Groningen*, No. 47.
_____. 1955, *Pub. Kapteyn Astr. Lab. Groningen*, No. 57.
_____. 1956, *Pub. Kapteyn Astr. Lab. Groningen*, No. 59.
van Rhijn, P. J., and Schwassmann, A. 1935, *Zs. f. Ap.*, **10**, 161.
Weistrop, D. 1972, *A. J.*, **77**, 849.
_____. 1976, *Ap. J.*, **204**, 113.
Westphal, J. A., *et al.* 1979, WF/PC GSFC Preliminary Design Review Package (CM-04), submitted to NASA.
Wielen, R. 1974, in *Highlights of Astronomy*, **Vol. 3**, ed. G. Contopoulos (Dordrecht: D. Reidel), p. 395.
Wildey, R. L., Burbidge, E. M., Sandage, A. R., and Burbidge, G. R. 1962, *Ap. J.*, **135**, 94.
Wills, D. 1978, *Phys. Scripta*, **17**, 333.
Young, P. J. 1976, *A. J.*, **81**, 807.
Zwicky, F. 1933, *Helvetica Phys. Acta*, **6**, 110.

JOHN N. BAHCALL and RAYMOND M. SONEIRA: Institute for Advanced Study, Princeton, NJ 08540